République **A**lgérienne **D**émocratique et **P**opulaire

Ministère de l'**E**nseignement **S**upérieur et de la **R**echerche **S**cientifique

Université 20 août 1955-Skikda

Faculté des Sciences

Département de Physique

N° : ……

Mémoire de Master

Filière : Physique

Spécialité : Physique des rayonnements

Thème

Simulation of clathrate-based solar cells

Présenté par :

Bouchareb Manal

Soutenu le :03/07/2023 devant le jury composé de :

S. Chaguetmi	Pr.	Université de skikda	Présidente
A. Chettah	Pr.	Université de skikda	Rapporteur
S. Labiod	MCA	Université de skikda	Examinateur

Année Universitaire : 2022/2023

Dedication

Every challenging work needs self-efforts as well as guidance of elders

Especially those who are very close to our hearts.

To begin with, I thank Allah for giving me power, ability and self-confidence to accomplish this research.

I dedicate this work to my dearest Father '***Djamel***' and Mother '***Zineb***' who were always beside me and supported me. Thank you for all you have done for me.

Special thanks to my brothers '***Chamsse Eddine***' and '***Aymen***' for their encouragement and motivation. Without forgetting my sweetest sisters '***Houda***', '***Aya***' and '***Roumaissa***'. I want you to know how much I appreciate you and how grateful I am for you. By the most sincere feelings and best words emanating from the heart, I dedicated this work to my aunts and uncles who stood with me in my tough circumstances, I give my special thanks and gratitude to all the ones who were with me.

B. Manal

ACKNOWLEDGMENTS

I want to express my deep appreciation to ***Dr. A. Chettah***, my model teacher and supervisor, for his invaluable assistance in helping me accomplish my academic work. He has been there to show me the right path whenever I made mistakes, putting in his best efforts to ensure the success of my project. I am truly grateful for his guidance, inspiration, and unwavering support.

I would also like to extend my sincere thanks to the board examiners, **Dr. S.Chaguetmi** and **Dr. S.Labiod**, for their valuable evaluation. Their willingness to dedicate their precious time to read and assess my work is greatly appreciated.

Additionally, I want to thank **MT. Bouzenzana** for his continuous support and assistance during my educational career. His guidance and help have played a vital role in my academic journey.

At last, I am immensely thankful to all my teachers who have provided me with valuable information and knowledge throughout my studies.

Table of contents

Table of contents

Table of contents

Liste of figures

Chapter I : General review of solar cells and Clathrates

Chapiter II : Solar Cell Capacitance Simulator (SCAPS)

Chapter III : Results and Discussion

Liste of figures

Liste of tables

Chapter II : Solar Cell Capacitance Simulator (SCAPS)

Chapter III : Results and Discussion

.

Introduction

Introduction

Introduction

Power is a crucial element in meeting the daily requirements of the modern world. To fulfill our energy needs, we primarily rely on fossil fuels, specifically oil and coal, which serve as the primary sources of energy. Together, they account for approximately 60-80% of our energy production. Nevertheless, the availability of fossil fuels is severely limited, necessitating significant investments in extraction and refining processes, which incur substantial costs.

The solar panel has become a more recent and comparatively environmentally friendly energy option that is both sustainable and cost-efficient when produced on a larger scale. Presently, efforts are focused on creating economically viable and highly efficient photovoltaic devices that generate electricity without material degradation.

Silicon-based solar cells have held a dominant position in the market for an extended period. However, their manufacturing and production necessitate sophisticated fabrication techniques, which contribute to the high cost of solar panels. As manufacturing capabilities have improved, there is a growing recognition of the value of thin film solar cells. Thin film technology offers economic advantages over other methods because it uses less material and incorporates different types of light-absorbing semiconductor materials.

Recently, a new solar cell structure has been fabricated including an inorganic clathrate n-type semiconductor layer (ITO/Ag/n-Si_{136}/p-Si/Al). Despite the weak response to light observed in the experimental measurement of the electrical current of this solar cell with thickness of 1 µm of the clathrate layer, it is still valuable to examine the effects of various parameters, including the thickness of the clathrate layer and its doping concentration.

Numerical modeling can play a significant role in enhancing our understanding of device characteristics, allowing researchers to model different device structures and save time and costs. In this study, numerical modeling was employed to estimate and analyze the impact of various physical parameters, such as absorber, buffer, and window layer thicknesses, doping concentrations, temperature, and solar illumination power, on device performance on the said clathrate-based solar cell. The device modeling was conducted using a dedicated simulation software called "Solar Cell Capacitance Simulator" (SCAPS-1D). Initially, a simple CIGS-based solar cell structure, consisting of Mo/CIGS/CdS/ZnO/FTO, was analyzed, in order to familiarize with the software. After that we moved to the clathrate-based solar cell and we used

the same procedure to estimate and analyze the impact of various physical parameters on the device performance.

The proposed results will give a valuable guideline for the feasible fabrication and designing of high-power conversion efficiency solar cells.

This dissertation is organized in three chapters besides a general introduction and conclusion.

Chapter one gives a general review of solar cells and group-II inorganic clathrates.

Chapter two describes the simulation tool ‘SCAPS-1D’ (Solar Cell Capacitance Simulator).

Chapter three reports the simulation results along with their interpretation in both cases: The CIGS-based solar cell and clathrate-based solar cell.

Chapter I

General review of solar cells and Clathrates

I.1. Semiconductor:

Semiconductors are the materials having electrical properties in between of conductor and a good insulator [1].

A semiconductor material in its pure form is neither a good insulator nor a good conductor. In terms of energy bands, semiconductors have an empty conduction band and almost filled valence band having very small forbidden energy gap as shown in Fig I.1. n

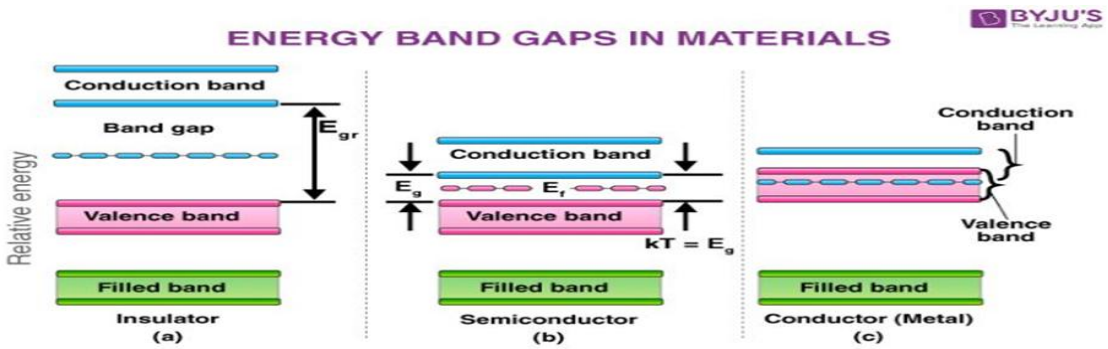

Fig I.1: Energy band gaps in materials, (a) Insulator, (b) Semiconductor, (c) conductor.

At 0 K temperature, conduction band have no electrons whereas valence band is completely filled. With the increase in temperature, the width of the forbidden gap decreases. Therefore, some of the valence electrons jump into the conduction band (leave a positive holes). This means that the conductivity of a semiconductor is increased with temperature. [2] They can be a single element like Ge and Si, a compound like InP, $GaAs$, $CdTe$ or alloys. Elemental semiconductors are characterized by atoms with four valence electrons. More common semiconductor materials are given in the periodic table (column 14) Fig I.2.

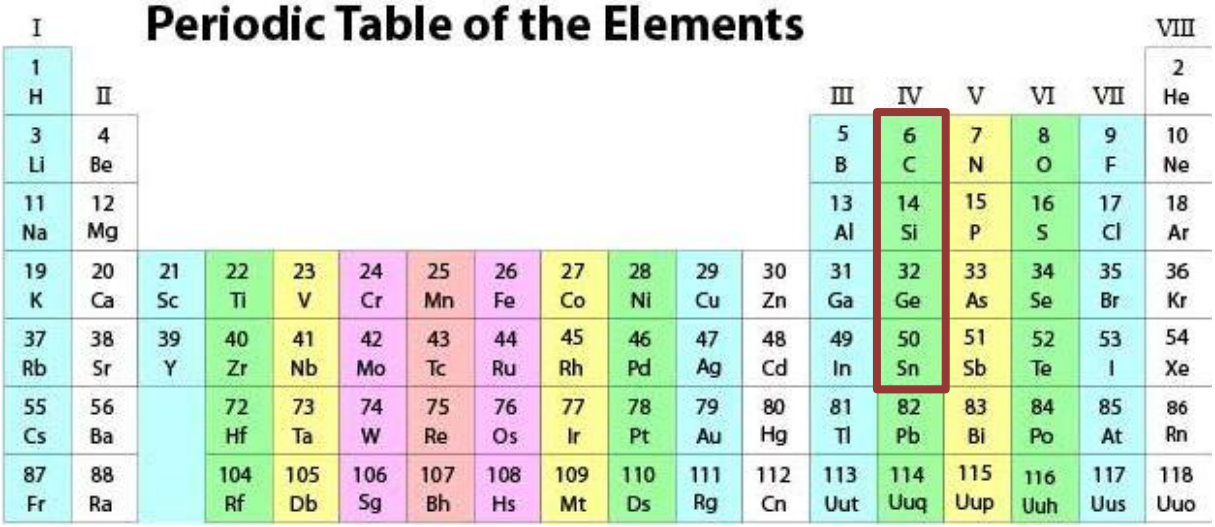

Fig I.2: Semiconductor materials in the periodic table

Semiconductors can be classified into intrinsic and extrinsic semiconductors. Intrinsic semiconductor allows a very small amount of current due to high resistance. Conducting ability can be considerably altered by adding certain impurities in intrinsic semiconductors. Semiconductors in which impurities are added are known as extrinsic semiconductor materials. The electrical conductivity of extrinsic semiconductors is higher than intrinsic semiconductors. Therefore, extrinsic semiconductors are used for the manufacturing of electronic devices such as diodes and transistors. Two types of impurities are added in intrinsic semiconductors to form extrinsic semiconductors. They are pentavalent and trivalent materials. Pentavalent materials have five valence electrons in their outermost orbit like in antimony (Sb), phosphorus (P) and arsenic (As). Whereas trivalent material has three valence electrons in their outermost orbit like indium (In), boron (B), aluminum (Al) and gallium (G).

I.2. P-N Junction

A P-N junction is interface or a boundary between two semiconductor material types, namely the p-type and the n-type, inside a semiconductor. In a semiconductor, the P-N junction is created by the method of doping. The p-side or the positive side of the semiconductor has an excess of holes, and the n-side or negative side has an excess of electrons. [3]

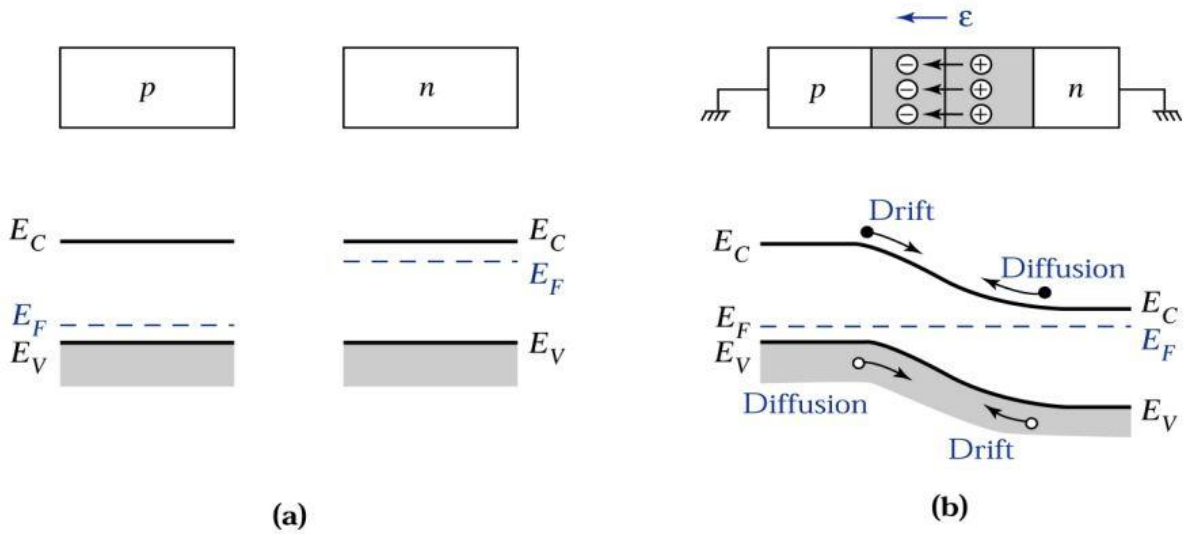

Fig I.3: (a) Uniformly doped p-type and n-type semiconductors before the junction is formed. (b) The electric field in the depletion region and the energy band diagram of a p–n junction in thermal equilibrium.

In Fig I.3(a), we see two regions of *p*- and *n*-type semiconductor materials that are uniformly doped and physically separated before the junction is formed. Note that the Fermi

level E_F is near the valence band edge in the *p*-type material and near the conduction band edge in the *n*-type material. While *p*-type material contains a large concentration of holes with few electrons, the opposite is true for *n*-type material.

When the p- and n-type semiconductors are jointed together, the large carrier concentration gradients at the junction cause carrier diffusion. Holes from the p-side diffuse into the n-side, and electrons from the n-side diffuse into the p-side. As holes continue to leave the p-side, some of the negative acceptor ions (N_A^-) near the junction are left uncompensated because the acceptors are fixed in the semiconductor lattice, whereas the holes are mobile. Similarly, some of the positive donor ions (N_D^+) near the junction are left uncompensated as the electrons leave the n-side. Consequently, a negative space charge forms near the p-side of the junction and a positive space charge forms near the n-side. This space charge region creates an electric field that is directed from the positive charge toward the negative charge, as indicated in the upper illustration of Fig I.3(b). The electric field is in the direction opposite to the diffusion current for each type of charge carrier. The lower illustration of Fig I.3(b) shows that the hole diffusion current flows from left to right, whereas the hole drift current due to the electric field flows from right to left. The electron diffusion current also flows from left to right, whereas the electron drift current flows in the opposite direction. Note that because of their negative charge, electrons diffuse from right to left, opposite to the direction of electron current.[4]

I.3. Solar radiation

Solar radiation is the energy emitted by the surface of the sun, which is sent in all directions through space as electromagnetic waves. This energy influences atmospheric and climatological processes.[5] The electromagnetic radiation spectrum, shown in Fig I.4, represents the complete range of wavelengths of electromagnetic radiation: from the longest radio waves through visible light and all the way to the shortest gamma rays. Due to its extremely high temperature and the energy it radiates, the sun emits short wave radiation.

Once it reaches the Earth's atmosphere, it gets absorbed by clouds and the surface. The ground heats up and re-emits energy. The earth being cooler than the sun, it emits long wave radiation in the form of infrared rays. In contrast to long wave radiation, short wave radiation

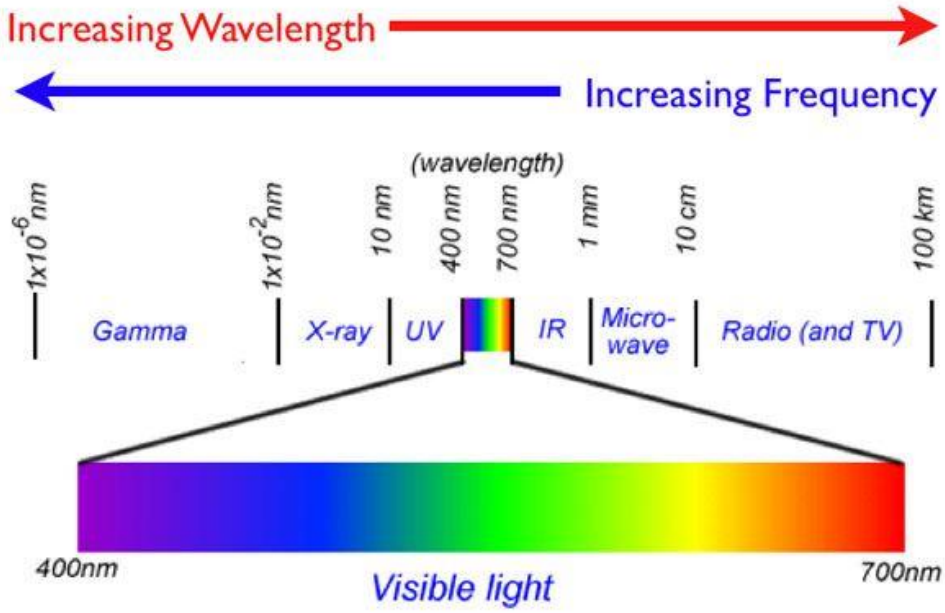

Fig I.4: Electromagnetic radiation Spectrum

has shorter wavelength and therefore higher frequency and energy. When it enters our atmosphere, it gets absorbed by numerous atmospheric components and the solar energy that reaches the ground is in the range [0.3 - 4]μm and lies party in the ultraviolet (UV) range, visible range and infrared (IR) range.[6]

I.4.Physics of solar cell

I.4.1. Photovoltaic effect

The term "photovoltaic" is composed up from the Greek words "phos" meaning light and "voltaic" meaning electricity, associated with Italian physicist name, Alessandro Volta. Electricity can be produced from the “photovoltaic effect”. A proper definition of the photovoltaic effect is the direct conversion of electromagnetic light radiation into electrical energy. The device used for the conversion of sunlight into usable electrical energy is known as a solar cell. Sunlight is an input source. The solar cells are also known as photovoltaic cells. It transforms sunlight into electricity. When sunlight falls on the photovoltaic cell then electrons freely move in a semiconductor material. If wires are connected to the positive and negative points of a photovoltaic cell, electron started to flow that is electricity and can be used to power an electric load.[7]

I.4.2. Working principle of photovoltaic cell

Photovoltaic cell working principle is based on the photovoltaic effect. Which is the formation of a potential difference due to electromagnetic at the junction of two different materials. This effect is closely related to the photoelectric effect, where the emission of electrons from a material is due to light absorption with a frequency above a material-dependent threshold frequency. This effect was explained by the scientist Albert Einstein in 1905 by assuming that the light comprises of well-defined energy quanta, called photons. The energy of such a photon is:

$$E = h\,\nu \tag{I.1}$$

Where $\nu = c/\lambda$ and c is the speed of light in a vacuum ($c = 3 \times 10^8\ m/s$), h is the Planck's constant ($h = 6.626 \times 10{-}34\ Js$) and ν is the frequency of the light. For the explanation of this effect, Einstein received the Nobel Prize in Physics in 1921. The photovoltaic effect can be divided into the following three basic processes [8]. first, is Generation of charge carriers due to photon absorption, secondly separation of photogenerated charge carriers and third Extraction of photogenerated charge carriers.

I.4.3. Equivalent circuit of solar cell

To understand the working principle of a solar cell, it is appropriate to make a model which is electrically equivalent. The ideal solar cell simplest model is given in Fig I.5 and consists of a constant current source and parallel connected diode. Constant current source works like a generator to push the electrons to the external circuit. Photocurrent I_L is generated due to the photovoltaic effect. Photocurrent depends on the intensity of the available sunlight, I_L of a current source is directly proportional to solar radiation. It means that with an increase of intensity of available sunlight, I_L must be increased. I_D is the reverse saturation current of a solar cell [9].

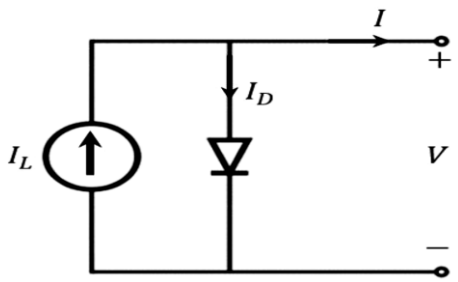

Fig I.5: Ideal solar cell

Practically photovoltaic cells are not ideal. So, shunt and series resistance components are added to the equivalent circuit. The subsequent equivalent circuit is given in Fig I.6

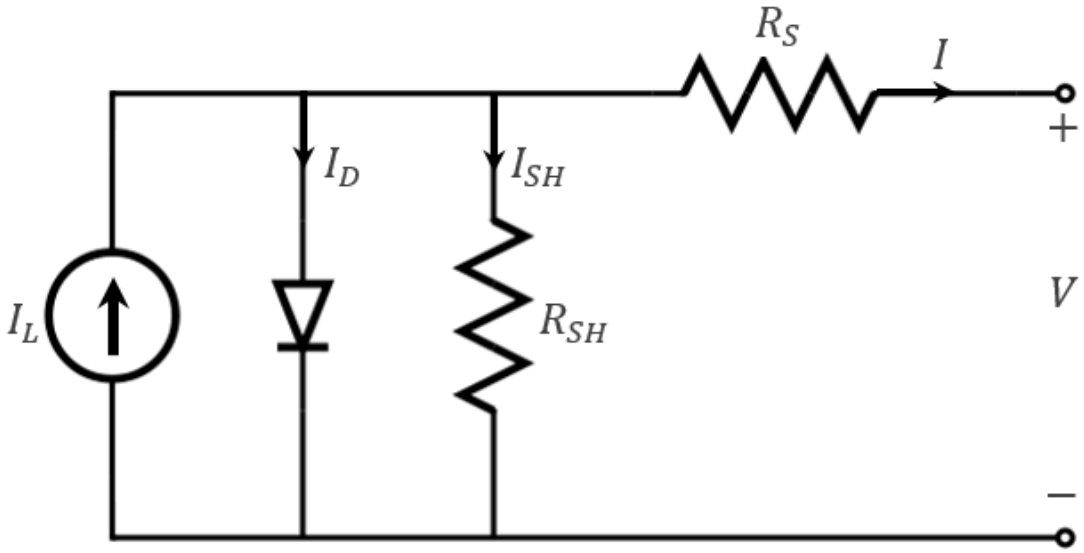

Fig I.6: Photovoltaic cell equivalent circuit

I.4.4 VI characteristic of a photovoltaic device

VI characteristics curve is the graphical representation of the operation of a photovoltaic cell. It can be well understood by considering the equivalent circuit of a solar cell. VI characteristic of a photovoltaic cell is the superposition of the VI curve of a device in darkness (absence of light) and illuminating (under light) conditions [10 11]. In dark conditions photovoltaic cell has similar electrical characteristics as of large diode. When light falls on the photovoltaic cell, electrical power can be extracted and VI curve down into the fourth quadrant. Amount of shift is directly proportional to the incident light intensity on a solar cell as shown in Fig I.7 Where maximum power is indicated by the shaded area. Illuminated cell added with diode dark currents, diode law becomes:

$$I=I_L - I_0 \left[\exp\left(\frac{qV+qR_sI}{nkT}\right) - 1\right] - \frac{V+R_sI}{R_{sh}} \quad (I.2)$$

where I_0 = diode leakage current under dark or dark saturation current, I_L= light generated current, V= applied terminal voltage across diode, q = electronic charge, k= Boltzmann's constant n = ideality factor and T= temperature

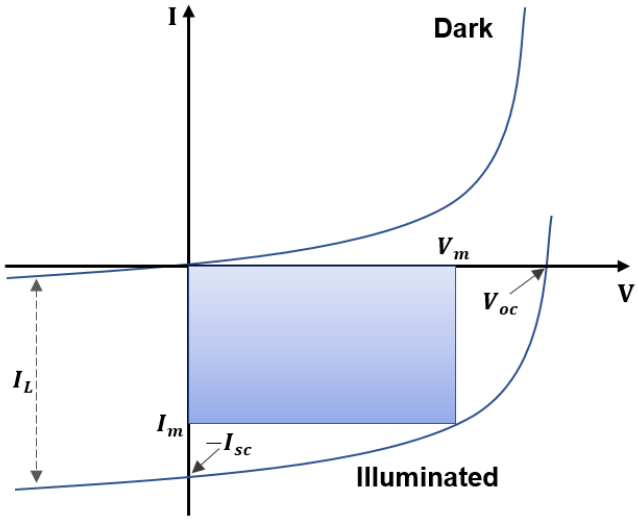

Fig I.7: VI characteristic of photovoltaic cell under illuminated and dark.

I.5. Basic parameters and electrical characterization methods

I.5.1. Short circuit current

The maximum current flow through the solar cell at zero load condition (at $R_L = 0$) or short-circuited is known as short-circuit current (I_{sc}). At the largest value of I_{sc}, the voltage of a solar cell will be zero [12]. The flow of I_{sc} is due to the collection and generation of light generated carriers. It mainly depends on the number of incident photons as well as the spectrum, area of solar cell, optical properties and the collection probability of light generated carriers. The graphical representation of I_{sc} is given in Fig I.8.

$$\text{Isc} = I_L - I_0 \left(\exp\left(\frac{qR_sI}{nkT}\right) - 1\right) - \left(\frac{R_sI}{R_{sh}}\right) \quad \text{(I.3)}$$

I.5.2. Open circuit voltage

The maximum voltage is taken from the solar cell (at $R_L = \infty$), which is known as open circuit voltage (V_{oc}). When a solar cell is an open circuited, and no load is connected across the solar cell then current will be at its minimum (zero) value, whereas the voltage will be at maximum value [13]. From solar cell equation, V_{oc} can be derived by setting net current to zero and is given in equation (I.4)

$$V_{oc} = R_{sh}\left(I_L - I_0\left(\exp\left(\frac{qR_sI}{nkT}\right) - 1\right)\right) \; at \; I = 0 \quad \text{(I.4)}$$

From the above equation, it is clear that open circuit voltage depends on I_0 (saturation current) and I_L (light generated current). I_0 depends on recombination in the solar cell. Therefore, V_{oc} is a measure of the amount of recombination in a solar cell. The graphical representation of open circuit voltage is given in Fig I.8.

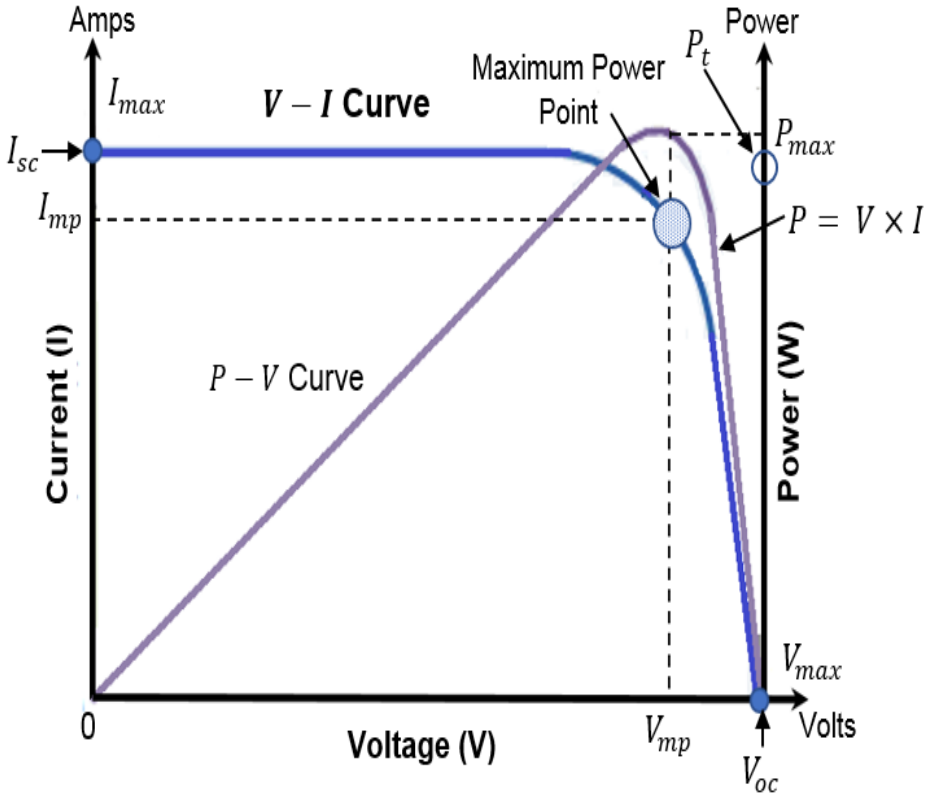

Fig I.8: I_{sc} and V_{oc} representation in VI curves

I.5.3. Fill factor

The measure of a photovoltaic cell quality is fill factor (FF), which is derived by equating the maximum power (P_{max}) to the theoretical power (P_t). Where power (P_t) would be output at both the open circuit voltage (V_{oc}) and short-circuit current (I_{sc}) as given in equations (I.5) and (I.6) [14]. Fill factor can be interpreted graphically as the ratio of the rectangular areas depicted in Fig.I.8.

$$FF = P_{max}/P_t \tag{I.5}$$

$$FF = \frac{\text{Vmax Ima}}{\text{Voc Isc}} \tag{I.6}$$

I.5.4. Maximum power

The output power of a solar cell is given in watts and is equal to the product of voltage times the current and is defined as

$$P_{out} = V_{out}\, I_{out} \tag{I.7}$$

Under short and open circuit conditions, no power is generated. The power output will be zero if both or anyone will be zero. The device will provide maximum power for maximum values of voltage and current.

$$P_{max} = V_{max}\, I_{max} \tag{I.8}$$

In terms of fill factor maximum power is by putting equation (I.6) in (I.8) we get

$$P_{max} = V_{oc}\, I_{sc}\, FF \tag{I.9}$$

I.5.5. Power conversion efficiency

Power conversion efficiency is the most frequently used parameter to relate the performance of two solar cells, and it is termed as PCE. It is defined as the ratio of output power from a solar cell to the input power from the sun [13].

$$\mathbf{PCE} = \frac{\boldsymbol{P_{max}}}{\boldsymbol{P_{in}}} \tag{I.10}$$

Where $$\boldsymbol{P_{max} = V_{oc}\, I_{sc}\, FF} \tag{I. 11}$$

And $$\boldsymbol{P_t = V_{oc}\, I_{sc}}$$

Therefore, from equation (I.10) and (I.11) the product of theoretical power (P_t), and fill factor (FF), divided by power the energy input from the sun is the power conversion efficiency [15]. Mathematically expressed in equation (I.12).

$$\boldsymbol{PCE} = \frac{\boldsymbol{V_{oc} I_{sc} FF}}{\boldsymbol{P_{in}}} \tag{I.12}$$

PCE depends on the parameters like incident sunlight intensity, solar cell working temperature and spectrum type. Thus, to compare two or more solar cells, it is important to carefully control the conditions under which PCE is measured. Typical measurement setup for terrestrial solar cells is with an $AM1.5G$ spectrum at a temperature of $25°C$.

I.5.6. Quantum efficiency

The quantum efficiency (QE) is the ratio of the extracted free charge carriers by the solar cell to the number of incident photons. In other words, QE relates to the response of a solar cell to different wavelengths. It may be given either as a function of energy or wavelength. The QE will be unity at the precise wavelength if all certain wavelength photons are absorbed and the resulting minority carriers are collected.[16]

I.6. Solar cell

The photovoltaic cell or solar cell is an electronic device, which converts solar radiation into electrical energy. The working principle is based on the photovoltaic effect. Practically for the photovoltaic energy conversion of solar radiation, semiconductor materials are used in a form of p-n junction. The structure of a solar cell can be well understood from Fig I.9. The basic steps in the operation of a solar cell are:

1. Generation of photogenerated carriers
2. Generation of current via collection of photogenerated carriers.
3. Generation of a large voltage across the solar cell.
4. Power dissipation at the load.[17]

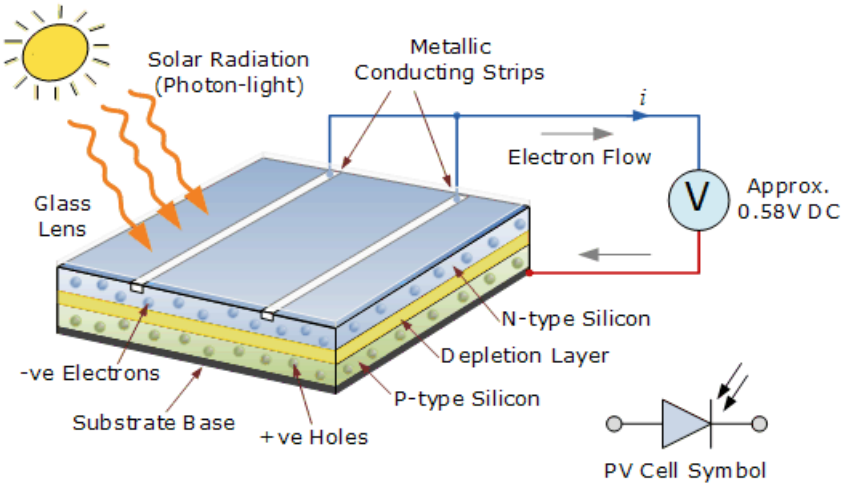

Fig I.9: Cross section of a solar cell

In Fig I.9 silicon-based solar cell is taken for a better understanding of the construction and working operation of a typical photovoltaic cell. p-type silicon works as an absorber layer and n-type silicon as a window layer. p-type silicon has the positively charged majority carriers known as holes whereas n-type silicon has negatively the charged majority carriers known as

electrons. Both sides of solar cells have conductive surface named as back metal contact and the front metal contact. Photogenerated current flows through external circuit by using these front and back metal contacts. When solar radiation or photo light falls on the solar cell, carriers (holes and electrons) are generated. These generated carriers are also known as photogenerated carriers and moves towards their respected layers and metal contacts. Due to this, output voltage appears across the solar cell. If we connect the load or any measuring instrument, current flow will start [17].

I.7. Different types of solar cells

Solar cells are divided into two major groups. They are silicon semiconductor type and non-silicon type. The details are as follows.

I.7.1. Silicon semiconductor type solar cells

There are three major types of silicon semiconductor photovoltaic cells, which are used to create panels.

Mono Crystalline Poly Crystalline Thin film

Fig I.10: Types of photovoltaic solar cells

I.7.1.1. Monocrystalline solar cell

These types of solar cells belong from first-generation solar cell technologies. The width of the wafer used in these types of solar cells is up to 200μm. The cell slice is cut from a pure silicon bar, which allows them to more efficiently converting the sunlight radiation energy into electrical energy. Silicon used in monocrystalline is single-crystal silicon. The complete cell is aligned in the same direction, so when the light falls on the cells at the accurate direction, they are very efficient. In a sunny day, photovoltaic cells work best with the sunlight directly falls on accurate direction. They are absorbing most of the solar radiation, so they have a uniform blacker color. Cost of the production of these types of solar cells is more than in the comparison

of a polycrystalline cell. In a comparison of polycrystalline, monocrystalline is the most efficient type of photovoltaic solar cells.

I.7.1.2. Polycrystalline solar cell

These types of solar cells also belong from first-generation solar cell technologies. These cells are made up of several silicon cells joined together instead of using a single crystal of silicon. In general, the cost of production of a polycrystalline solar cell is not much higher than monocrystalline. Therefore, they are also more affordable. In comparison with a monocrystalline solar cell, the power conversion efficiency of polycrystalline solar cell is less. Their overall manufacturing design can often make up for the efficiency loss.

I.7.1.3. Amorphous solar cell

Amorphous silicon ($a-Si$) solar cells belong from a thin-film solar cell. In these types of solar cells, one or more layers of photovoltaic materials are deposit on a substrate. In comparison with other technologies, they have low manufacturing cost. To make thin-film photovoltaic solar cells, manufacturers spray a layer of silicon on a substrate. They are produced by placing one or more thin layers of photovoltaic composite on a substrate. Thin film photovoltaic solar cells are different from other types; they are also more flexible than other types. It can be put onto different surfaces i.e. curved and straight.

I.7.2. Other types of solar cell

Above discussed, silicon-based solar cells are most commonly used solar cells. There are some other types such as ($CIGS$) and cadmium telluride ($CdTe$) based solar cells, kesterite and perovskite solar cells, which are also used due to their good conversion capabilities, earth-abundant materials, and enhanced power conversion efficiencies. [18]

I.8.Clathrate :

I.8.1.What is clathrate?

The term ‘Clathrate’, which means ‘inclusion’ or ‘cage-like material’, is derived from the Greek word ‘Klethra’ originally meaning ‘alder’ [19]. It was first used by Powel in 1948 in his works on organic inclusion compounds as β-quinol [20]. That term was extended to describe solid gas hydrates in 1952 by Pauling and Marsh [21], (Linus Pauling was awarded the Nobel prize of chemistry in 1954 for his works). Since then, the term clathrate was adopted to describe

any material whose main lattice is formed by cage-like framework that encloses guest atom or molecule within. Fig I.11 illustrates a hydrate clathrate where the framework is formed by H_2O molecules arranged in a way to form a cage-like structure, and CH_4 methane molecules are entrapped inside the framework [22]. The main characteristics of clathrate compounds are:

(1) The unit-cell is usually large, highly symmetrical and the lattice constants almost independent of the nature of the guest species, which can be an atom or a molecule.

(2) The host lattice itself can be considered as a possible allotropic form of the major species, which is stabilized by the presence of guest species.

(3) The guest lattice can be non-stoichiometric and even guest-free clathrates exist.

(4) At high temperature, they decompose into the starting chemical species, and correspond to a kind of association rather than a combination.

(5) The host-guest interactions affect the properties of clathrates. They are generally weak as in clathrate hydrates, but they can be stronger as in inorganic clathrates.

Several families of clathrates are known, the host lattice of which are of inorganic or organic nature. The most important and representative of them is the series of the so-called gas and liquid hydrates, in which the host lattice is made of corner sharing H_2O tetrahedrons forming large cages of 20 to 36 vertices, in which are enclosed guest molecules of a gas (Cl_2, SO_2, CH_4, H_2S, Kr, etc.), or a liquid (C_6H_6, CH_3I, CH_3Cl, CH_2Cl_2, $CHCl_3$, CCl_4, etc.).

I.8.2. A little history of inorganic clathrates

In 1811 H. Davy reported the first evidence of a compound of water cage-like structure containing chlorine gas molecules, the compound will be later known as a ***hydrate clathrate*** [23]. In 1823 Michael Faraday successfully determined a composition for this compound and reported it as $(Cl_2)1(H_2O)_{10}$[24]. It was only after the introduction of x-ray diffraction, and more than a century later (1951), that the crystalline structure of this compound was determined. Claussen [25] and Pauling & Marsh [21] independently determined that hydrate clathrate of chlorine was in fact built of a hydrogen-bonded network of water, with the oxygen atoms forming cage-like networks within which chlorine atoms are confined as "guests". The correct stoichiometry was determined as $(Cl_2)1(H_2O)_8$ [26]. Today, the word clathrate is used to describe compounds, which display a host-guest relationship.

In 1965, it was observed that the x-ray diffraction patterns resulting from the thermal degradation of certain silicides were similar to those of ice clathrates: an observation that led to the discovery of a new class of clathrates formed of tetrahedrally bound silicon [27]. Inspired from hydrate clathrates, Group-IV clathrates, and precisely silicon-based clathrates are the most studies and promising clathrates as they exhibit a variety of possible technological interest as well as the wide range of possible introduction of many atomic species, thus, type-II clathrates with the chemical formula Na_xSi_{136}, were the first silicon clathrates to be synthesized in 1965 by two French groups, i.e. Cros et al [28] and Kasper et al [29]. This class of materials encountered small amount of interest until the mid-1990s were exceptional superconducting and semiconducting properties were discovered [30].

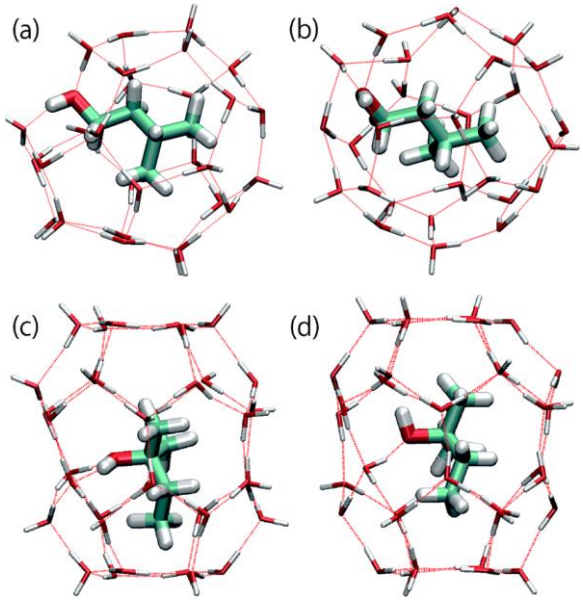

Fig I.11: Snapshots of the $5^{12}6^4$ cages in sII and $5^{12}6^8$ cages in sH clathrate hydrates from the ab-initio MD simulations. The O–H group of 3-methyl-1-butanol molecules in sII hydrates is incorporated into $5^{12}6^4$ cages and forms hydrogen bonds with (a) two or (b) three water molecules. The O–H group of 2-methyl-2-butanol molecules in sH hydrates forms hydrogen bonds with (c) two or (d) one water molecules.

Silicon, germanium, tin and carbon are often discussed in comparison with each other in terms of the same group-IV elements. Since the discovery of carbon cluster C_{60} (fullerene), it has been expected that similar type of clusters should be prepared with silicon, germanium or tin. As a matter of fact, there are silicon clathrate compounds which are composed of silicon polyhedral analogous to fullerenes. Silicon clathrate compounds, M_xSi_{46} and M_xSi_{136} (M = Na,

Ba, K, Ca, Rb, Cs) were first prepared and extensively studied by Kasper *et al*. The compounds are composed of Si-*sp3* bonds with about the same bond distances and bond angles as in elemental diamond silicon, but the silicon tetrahedra build an open network having pentagonal dodecahedra (12 pentagonal faces, [5^{12}]), and tetrakaidecahedra (12 pentagonal faces and 2 hexagonal faces, [5^2 6^2], for MxSi46, and pentagonal dodecahedra ([5^{12}]) and hexakaidecahedra (12 pentagonal faces and 4 hexagonal faces, [5^{12} 6^4]) for type-II clathrate M_xSi_{136} [27].

I.8.3. Structures of some silicon clathrates

According to their composition, structures, the nature of their constituent cages and the way they associate, several types of inorganic clathrates can be distinguished. Theoretically, ten types of silicon clathrates can be classified, but only four types are realized experimentally, i.e. type-I, type- II, type-III and type-VIII.

I.8.3.1. Type-I clathrate

Type-I clathrate is the first know form of all clathrates, and with the formula X_8Si_{46}, (X=guest atom), is the most investigated clathrate, and to the date about 122 compound are known through the partial or complete substitutions of host or guest atoms. it was first synthesized in 1965 in its inorganic group 14 [27]. With formula X_8Si_{46}, while its hydrate counterpart analog was known, it was only reported in 1965 as mentioned above. Type-I clathrates crystallize in the Pm-3n space group (number 223), which presents a simple cubic unit cell. The main lattice of type-I clathrate structure is formed from association of dodecahedrons (twelve pentagonal faces with 20 atoms on edges [5^{12}]) with tetrakaidecahedrons [31]. Tetrakaidecahedra polyhedron are connected to each other by sharing their hexagonal faces and with other dodecahedrons by sharing their pentagonal faces, while dodecahedrons are connected to each other by sharing their.

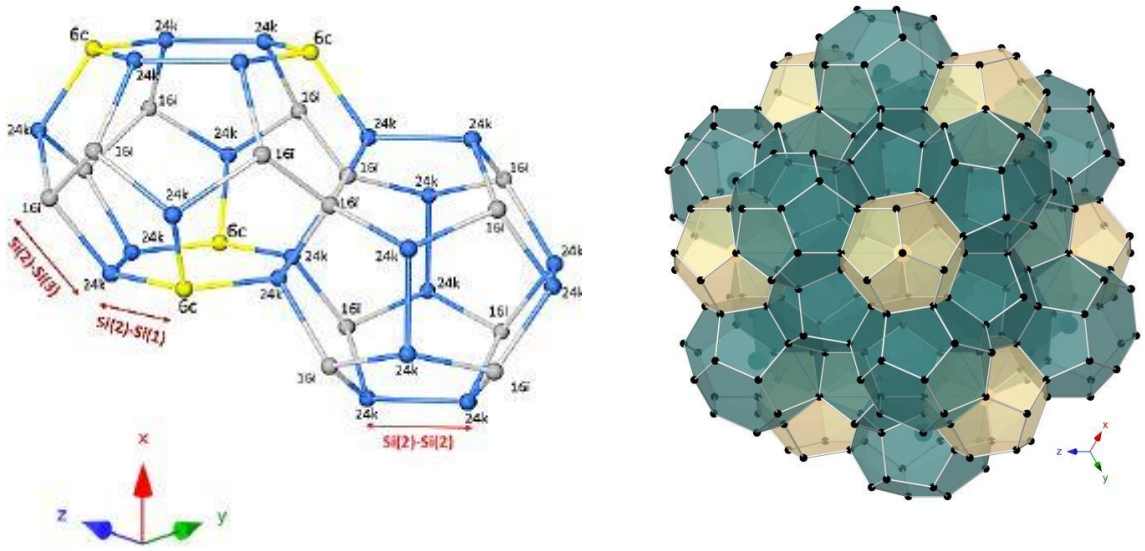

Fig I.12: Type-I Si clathrate is composed from the association of dodecahedral and tetrakaidecahedral cages [32].

I.8.3.2. Type-II clathrate

Type-II clathrates are initially composed from thorough associations of eight large hexakaidecahedra (28-vertex with 16 faces [$5^{12}6^4$]) together with sixteen pentagonal dodecahedra [5^{12}]. Type-II clathrates usually crystallize in the face-centered cubic FCC space group Fd3m. The hexakaidecahedra share all of their hexagonal faces forming a diamond-like 3D network (Fig I.13). Additionally, each hexakaidecahedron is encircled by twelve pentagonal dodecahedra, forming a truncated tetrahedron. Thus, the space is fully filled. The unit cell of type-II clathrate contains 16 small and 8 large polyhedra, with a generalized formula of X_6M_{24} or $X_{24}M_{136}$ (X is the guest atom and M is the group-IV host atom, Silicon in our case). Both cages can be filled with the same type of guest atoms, like Na, or with two different types of guests, like Na and Cs, with the larger cation occupying the larger cages [33]. So far, anionic type-II clathrate structures with frameworks based on Si, Ge, and Sn atoms have been reported [34, 35]. The relative ratio of the framework cage volumes to the guest cation radii determines which type of cages host the vacancies [36]. In the Na_xSi_{136} clathrates for example, for compositions with sodium content x less than 3, Na atoms tend to occupy the large hexakaidecahedral cages [$5^{12}6^4$] [37]. In contrary for Sn-based clathrate-II structures with Ba and K guests, only pentagonal dodecahedral cages [5^{12}] are occupied, and the hexakaidecahedra are not [38]. It is not uncommon for type-II clathrate structures to be partially filled, or even completely empty "guest-free". The guest-free type-II germanium clathrate Ge_{136} was described as new allotropic structure of germanium, and it was prepared by a mild oxidation of Na_4Ge_9 in

ionic liquids [39]. Additionally, an empty silicon-based clathrate-II with an extremely small residual Na content was prepared by annealing Na_xSi_{136} with iodine [40]. And a thin film of guest free type-II silicon clathrate was for the first time successfully grown over a Si(111) substrate by means of vapor deposition and subsequent heat treatment within iodine [41].

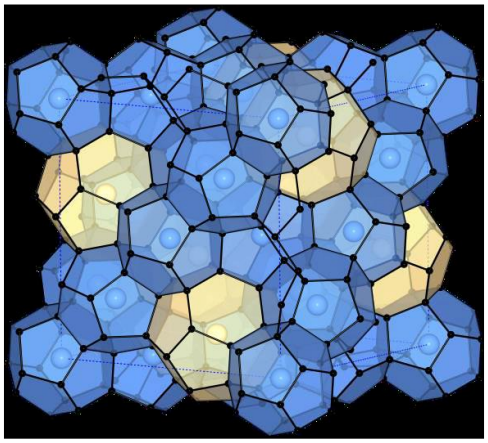

Fig I.13 Type-II silicon clathrate X_{48} Si_{136}

I.8.3.3. Type-III clathrate

The crystalline structure of type-III clathrate is composed from three types of polyhedra, i.e. ten dodecahedra [5^{12}], sixteen tetrakaidecahedra [$5^{12}6^2$], and four pentakaidecahedra [$5^{12}6^3$]. It crystallizes in the tetragonal space group P42/mnm. The tetrakaidecahedral cages form a sort of two distinct columns running along the <001> crystallographic direction (Fig I.14). The first type of column is made by the sharing of hexagonal faces. Whereas, the second type of column is made of the tetrakaidecahedra. After association of polyhedra, the remaining space will be filled by isolated pairs of either the pentakaidecahedra [$5^{12}6^3$] or the [5^{12}] dodecahedra. There are 172 host framework atoms in these clathrates, and their formulas can be generalized as $X_{30}M_{172}$. Similarly to the type-II clathrate, the cages in the type-III clathrate maybe filled with guests of different sizes or they may be partially vacant [36]. The first synthesis of two compounds of type-III clathrates were reported by *Bobev et al* in 2001 [34]. They have successfully synthesized and characterized a group with chemical formula of: $Cs_{30}Na_{(1.33x-10)}$-$Sn_{(172-x)}$ and $Cs_{13.8}(1)Rb_{16.2}(1)Na_{(1.33x-10)}Sn_{(172-x)}$ where $x\approx9.6$.

The two new compounds of ideal formula of $A_{30}Tt_{172}$ are found to be isostructural with inclusion compounds of the clathrate-III type such as $[(Br_2)20\blacksquare10](H_2O)_{172}$ and $[(CH_3OCH_3)20\blacksquare10]$- $(H_2O)_{172}$ where "■" denotes a vacancy [42]. These type-III clathrates exhibited a complete occupation of all of the polyhedral cages by Na alkali atoms and have

some vacancies in the Sn framework. In this structure, Na plays an unusual role when partially filling up the framework vacancies.

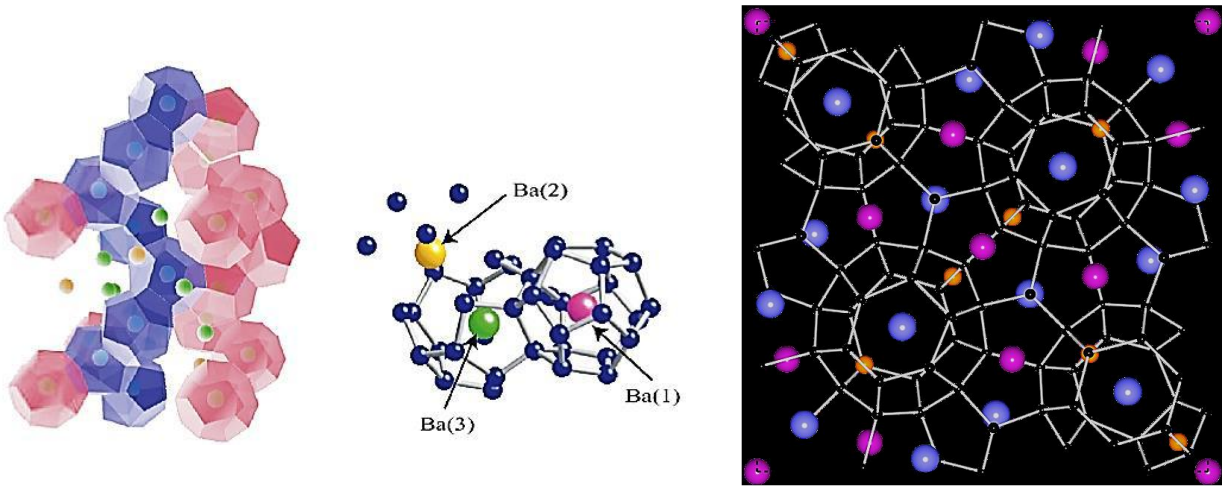

(a) (b)

Fig I.14: 3D polyhedral representation of type-III silicon clathrate Ba_{30} Si_{172} (a) by Tamegai *et al* [43] , (b) a (001) plane view.

I.8.3.4. Type-VIII

Type-VIII silicon clathrate with the same chemical formula as for the type-I phase (allotropic forms of the same clathrate compound), crystallizes in the body-centered cubic space group I4-3m (#217). The main framework of type-VIII clathrate is formed by combination of only one type of strongly-distorted dodecahedral cages (S_{23}), the host atoms of silicon occupy four Wyckoff positions: 2a, 12d, 24g and 8c, whereas, the guest atoms M occupy the 8c sites.

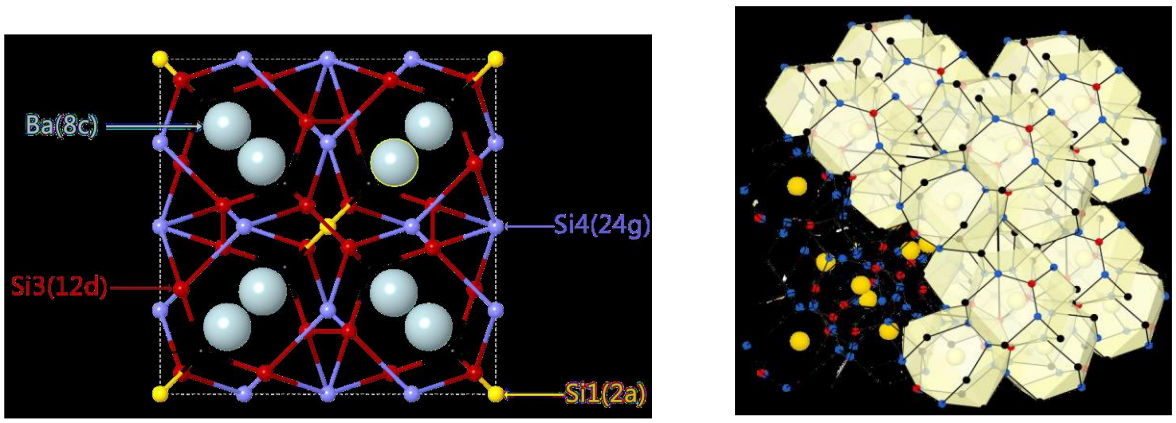

Fig I.15: shows the configuration of a unit cell of type-VIII M_8Si_{46} silicon clathrate [44].

Chapter II

Solar Cell Capacitance Simulator (SCAPS)

II.1. Photovoltaic device modeling tools

Principally solar cell modeling tool can be capable to solve the basic semiconductor equations such as Poisson equation and continuity equation. To simulate the realistic cells, the device modeling software must meet numerous additional requirements. They must be able to simulate multiple layers. Simulation tool should be able to give the response and correctly treats the recombination problem and, on an interface, and different layers defects. The modeling software must be able to calculate and simulate the electro-optical measurements under illumination and dark conditions, and this is not only JV characteristics but also the capacitance and spectral response. To measure and analyze the different solar cell parameters, numerous tools are available and efficiently used for device modeling. Engineers and researchers are using different types of photovoltaic simulation software's in their research centers and in universities [45]. Most commonly used software's are $SCAPS - 1D$ (Solar Cell Capacitance Simulator), $AMPS– 1D$ (Analysis of Microelectronics and Photonics Structures), $SILVACO\ TCAD, - HET$ (Automat FOR Simulation of HET erostructures), $PC1D$ and ASA (Amorphous Semiconductor Analysis)

We use $SCAP - 1D$ software for my research work because of the extensively available literature on PV device modeling and analyzing the performance.

II.2.Basic semiconductor equation

To analyze the performance of the solar cell, device simulation software must be able to solve the basic semiconductor equations. In device performance, these equations play a crucial role. The Poisson equation relating the charge to electrostatic potential is the governing equation. Poisson's equation for electrostatic potential (V) is given in equation **II.1** [46].

$$\frac{d^2V}{dx^2} = \frac{\rho q}{\varepsilon} \qquad \textbf{II.1}$$

Where ε is the product of permittivity of free space ε_0 and semiconductor dielectric constant ks i.e. ($\varepsilon = \varepsilon_0\ ks$) and ρ is the density of charge (C/cm^3) and. From charge neutrality equation ρ can be expressed as given in equation II.2 with an assumption that dopant is totally ionized.

$$\rho = (p - n + N_D^+ - N_A^-) \qquad \textbf{II.2}$$

Where q is electronic charge, p is concentration of holes, n is concentration of electrons, N_A^- ionized acceptor dopant carrier concentration and N_D^+ is ionized donor dopant carrier concentration. By putting equation II.2 in equation **II.1** it will become as equation II.3.

$$\frac{d^2V}{dx^2} = \frac{\mathrm{q(p - n + N_D^+ - N_A^-)}}{\varepsilon} \qquad \textbf{II.3}$$

and to solve equation **II.3** for V as a function position value of x one must have to rearrange the expression for the concentration of carriers (p, n). The second equation is a *continuity equation*, the reason that the continuity equation is called governing equation because drift, diffusion, generation, and recombination are analyzed simultaneously. Equation **II.4** and equation II.5 represent continuity equation for concentration change in electron and hole.

$$\frac{\partial n}{\partial t} = \frac{1}{q}\frac{\partial J_n}{\partial x} + (G - R) \qquad \textbf{II.4}$$

$$\frac{\partial p}{\partial t} = \frac{1}{q}\frac{\partial J_p}{\partial x} + (G - R) \qquad \textbf{II.5}$$

The output from equations **II.1**, **II.4** and **II.5** have non-linear dependencies on charge carrier concentration (p, n). Therefore, these equations will be solved with numerical techniques with standard approaches like the discretization of an equation, discretization of device and set of boundary conditions. To measure the current and characteristics of solar cell simulator must be able to solve drift-diffusion equation for current in a solar cell. The drift-diffusion equation of charge carriers is given in equation **II.6** and equation **II.7** [47].

$$J_n = -q\mu_n n\frac{\partial V}{\partial x} + qD_n\frac{\partial n}{\partial x} \qquad \textbf{II.6}$$

$$J_p = -q\mu_p p\frac{\partial V}{\partial x} - qD_p\frac{\partial p}{\partial x} \qquad \textbf{II.7}$$

J_n and J_p are the current densities for electron and holes, μ_n and μ_p are mobility of carriers, D_n and D_p are diffusion coefficient of electrons and holes and from Einstein relationship, the diffusion coefficient is depended upon the mobility of carrier with the product of carrier lifetime. Relation of D_n with the mobility of carrier is given in equation **II.8**.

$$D_{(n,p)} = \mu_{n,p}\frac{KT}{q} \qquad \textbf{II.8}$$

To find the solution for equations **II.3**, **II.4** and **II.5** other quantities needed like generation and recombination (G, R) and this can also be expressed as net recombination in a device (U). That is represented in equation **II.9** for n −type semiconductor.

$$U=\frac{p-p_0}{\tau_p} \quad \textbf{II.9}$$

II.3.SCAPS-1D

Solar Cell Capacitance Simulator ($SCAPS$) program developed at the University of Gent, Belgium is used to simulate the photovoltaic devices. Several researchers have contributed to its development such as Alex Niemegeers, Marc Burgelman, Koen Decock, Stefaan Degrave, Johan Verschraegen. $SCAPS-1D$ is the one-dimensional simulation program for the modeling of PV devices. Seven different semiconductor layers exclusive of back and front contacts are possible to take as input in $SCAPS-1D$ software. $SCAPS-1D$ tool is freely available for the photovoltaic research community and can be freely downloaded from its web link. It runs on a window operating system environment. This software is designed to simulate and helps us to analyze the $J-V$ characteristics curve, ac characteristics ($C-V$ and $C-f$), spectral response (QE) of a device, power conversion efficiency (PCE), fill factor (FF), short-circuit current (J_{sc}), open circuit voltage (V_{oc}), energy bands of materials used in solar cell and concentration of different material used by solving the semiconductor basic equations [48],[49],[50].

II.4.Parameters

Input physical parameters are the essential conditions for resolving the fundamental semiconductor equations in device modeling. The physical parameters used in $SCAPS-1D$ software for numerical analysis are

Parameters	Abbreviation	Unit
Layer Thickness	w	μm
Bandgap energy	Eg	eV
Conduction band effective density of states	N_c	cm^{-3}
Valence band effective density of states	N_v	cm^{-3}
Dielectric permittivity	ε_r	
Electron affinity	X	eV
Hole mobility	μ_p	cm^2/Vs
Electron mobility	μ_e	cm^2/Vs

Electron doping concentration	N	cm^{-3}
Hole doping concentration	P	cm^{-3}
Absorption coefficient	A	cm^{-1}
Bulk defect concentration	N_T	cm^{-3}
Capture cross-section	Σ	cm^2
Defect energy level	E_T	eV
Metal work function	Φ_M	eV

Table II.1. Physical parameters

All the simulations are conducted under 1.5AM solar radiation with the power density of 100 $mW/cm2$ is used as the illuminating source. Functional parameters of solar cells are given in the under table:

Parameters	Abreviation	Unit
Power Conversion Efficiency	PCE or η	%
Short circuit current	J_{sc}	mA/cm^2
Open circuit voltage	V_{oc}	v
Fill factor	FF	%

Table II.2. Functional parameters of solar cells

II.5.The basics

SCAPS is a Windows-oriented program, developed with LabWindows/CVI of National Instruments. SCAPS opens with the 'Action Panel'.

The meaning of the blocks numbered from 1 to 6 are the following: (see Fig.II.1)

1. Run SCAPS .
2. Define the problem, thus the geometry, the materials, all properties of your solar cell
3. Indicate the circumstances in which you want to do the simulation, i.e. specify the working point
4. Indicate what you will calculate, i.e. which measurement you will simulate.
5. Start the calculation(s)
6. Display the simulated curves.

This is further explained below.

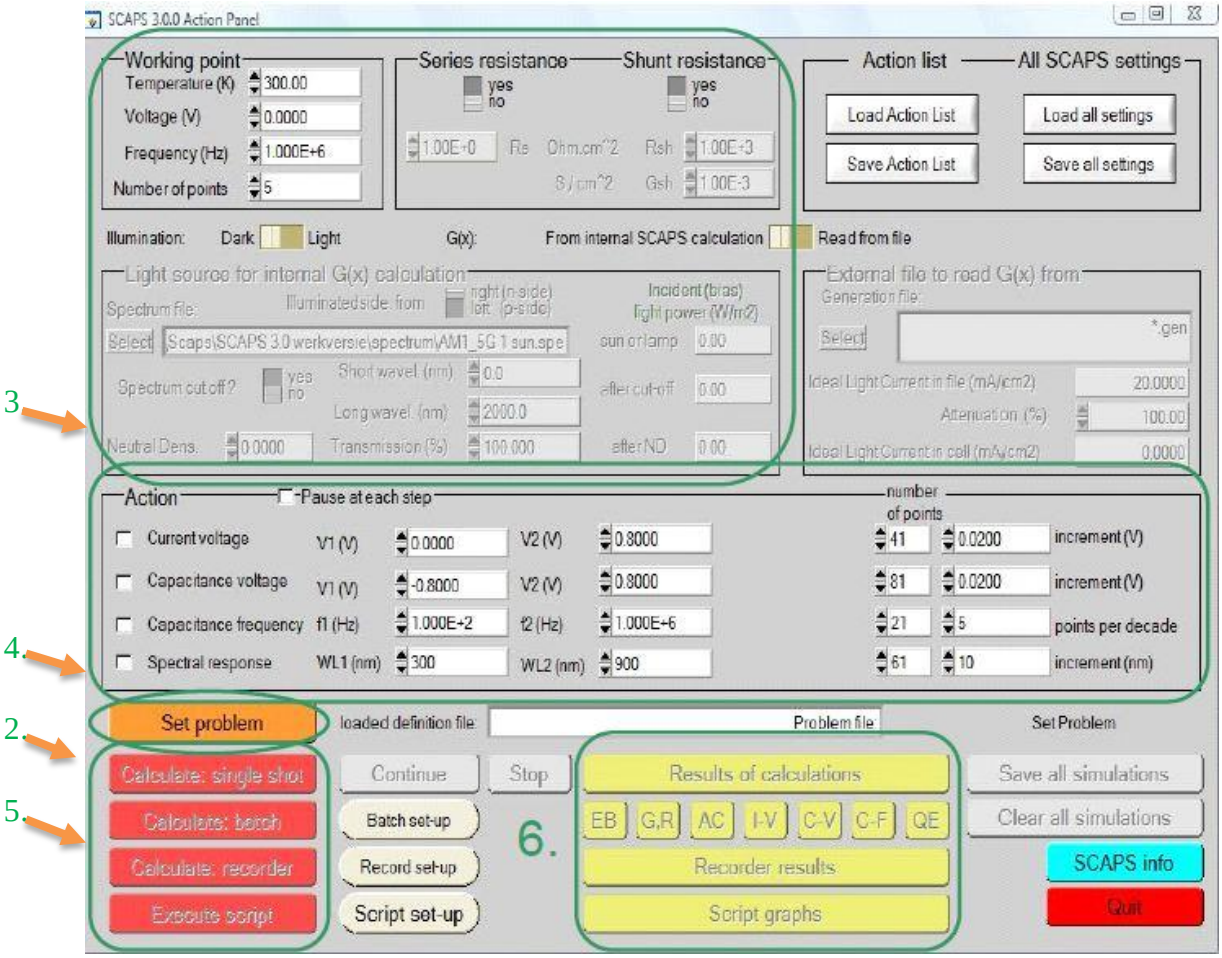

Fig II.1: The SCAPS start-up panel: the Action panel

II.5.1.Run SCAPS

Click the above pictogram on the Desktop, or double-click the file scaps3309.exe in the file manager (or any other SCAPS version). SCAPS opens with the Action Panel.

II.5.2.Define the problem

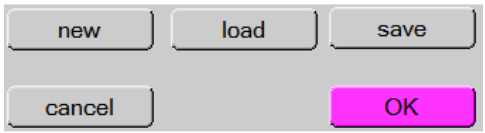

Click the button set problem in the action panel, and chose load in the lower right corner of the panel that opens. Select and open e.g. the file NUMOS CIGS baseline.def: that is the example problem file of the practicum session at the NUMOS workshop, Gent, 30 march 2007. This file is supposed to be in the folder /scaps/def, where /scaps/ stands for the directory where you installed SCAPS, and where the SCAPS .exe file resides. If necessary, browse to find this file. In a later stage, you can alter all properties of the cell by clicking set problem in the action panel.

II.5.3.Define the working point

The working point specifies the parameters which are not varied in a measurement simulation, and which are relevant to that measurement. Thus:

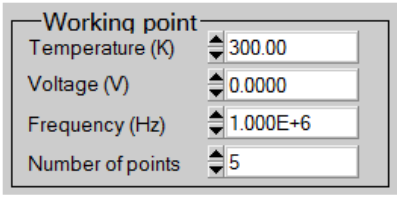

- the temperature *T*: relevant for all measurements. Note: in SCAPS, only $N_C(T)$, $N_V(T)$, the thermal velocities, the thermal voltage kT and all their derivatives are the only variables which have an explicit temperature dependence; you must input for each *T* the corresponding materials parameters yourself.

- the voltage *V*: is discarded in *I-V* and *C-V* simulation. It is the dc-bias voltage in *C-f* simulation and in $QE(\lambda)$ simulation. SCAPS always starts at 0 V, and proceeds at the working point voltage in a number of steps that you also should specify.

- the frequency *f*: is discarded in *I-V*, $QE(\lambda)$ and *C-f* simulation. It is the frequency at which the *C-V* measurement is simulated.

- the illumination: is used for all measurements. For the $QE(\lambda)$ measurement, it determines the bias light conditions. The basis settings are: dark or light, choice of the illuminated side, choice of the spectrum. A one sun (= 1000 W/m2) illumination with the 'air mass 1.5, global' spectrum is the default, but you have a large choice of monochromatic light and spectra for your specialized simulations. If you have an optical simulator at your disposal you can immediately load a generation profile as well in stead of using a spectrum.

II.5.4.Select the measurement(s) to simulate

In the action-part of the Action Panel, you can select one or more of the following measurements to simulate: *I-V*, *C-V*, *C-f* and $QE(\lambda)$. Adjust if necessary the start and end values of the argument, and the number of steps. Initially, do one simulation at a time, and use rather coarse steps: your computer and/or the SCAPS program might be less fast than you hope, or your problem could be really tough... A hint: in a *C-V* simulation, the *I-V* curve is calculated as well, no need then to specify it separately.

II.5.5.Start the calculation(s)

Click the button calculate: single shot in the action panel. The Energy Bands Panel opens, and the calculations start. At the bottom of the Panel, you see a status line, e.g. "iv from 0.000 to 0.800 Volt: V = 0.550 Volt", showing you how the simulation proceeds. Meanwhile, SCAPS stands you a free movie how the conduction and valence bands, the Fermi levels and the whole caboodle are evolving. When you see the hated divergence message, you are entitled

to get into a bad mood, but don't exaggerate. Anyway, you did not loose the *I-V* points already calculated.

II.5.6.Display the simulated curves

After the calculation(s), SCAPS switches to the Energy band panel (or the AC-band panel). You can now look at your ease to the band diagrams, carrier densities, current densities, at the last bias point calculated (stop your calculations earlier, or use the pause button on the Action Panel if you want to look at an intermediate state at ease). You can output the results (buttons print, save graphs, show (then the numbers are shown on screen; cut & paste to e.g. Excel is possible), or save (then the numbers are saved to a file). You can switch to one of the specialized output Panels (if you have already simulated at least one corresponding measurement). [51]

Chapter III

Results and Discussion

III.1.Introduction

In the framework of this dissertation, we aim to perform an optimization of a clathrate-based solar cell using the famous SCAPS-1D software. As a first step, and in order to familiarize with SCAPS, we use this software to optimize a well-known CIGS-based solar cell. The optimization includes varying many parameters, namely the thickness of the absorber layer, operating temperature and acceptors concentration and examine their influence on the I-V curve's main parameters (V_{0C}, J_{SC}, *FF* and η (eta)). In a second step, we apply the same procedure to the clathrate-based solar cell.

In this chapter, we report the different results obtained by SCAPS-1D and possible interpretations and conclusions.

III.2.General setting and parameters in SCAPS

III.2.1.Numerical setting

In the present work, all the numerical parameters (convergence setting, metastable update convergence setting, mesh generator setting, defect energy distribution settings,…) were set to SCAPS defaults.

III.2.2.Illumination spectrum

We have chosen the standard AM1.5 Global spectrum with an integrated power 1000 W/m^2 as the illumination spectrum in the whole calculations performed in the present work. For more information, refer to chapter I-…

III.2.3.Circuit resistance

In all the present calculations, we considered an ideal solar cell, i.e., the serie resistance Rs = 0 ohm and shunt resistance Rsh >> (infinity) in case of CIGS-based device. However, in the clathrate-based device we explored a wide range of values of series resistance.

III.2.4.Back and front contacts

They are considered Ohmic contacts having flat-bands approach.

III.3.Optimization of CIGS Based solar cell

As mentioned earlier, we first perform the modeling of a CIGS-based solar cell as defined in SCAPS-1D. Therefore, the cell configuration along with the parameters of the different layers are loaded from the software ("def" folder). The following section describes the cell configuration and the different parameters used in the calculation.

III.3.1.Configuration of the cell

The cell has the following configuration: Mo/CIGS/CdS/ZnO/FTO. The Mo (Molybdenum) layer serves as the back contact of the solar cell, which provides electrical contact and helps extract the generated electricity from the cell, and CIGS (p-type copper Indium Gallium Selenide) is the absorber layer of the solar cell, responsible for capturing sunlight and converting it into electrical energy. The CdS (n-type Cadmium sulfide) layer acts as the buffer layer and ZnO (n-type Zinc Oxide) layer is a thin film of zinc oxide that acts as the front contact in the solar cell structure. FTO (Fluorine-Doped Tin Oxide) layer is a type of transparent conducting oxide, which is used as front contact in solar cells. It provides electrical conductivity and enables light transmission to the underlying layers.

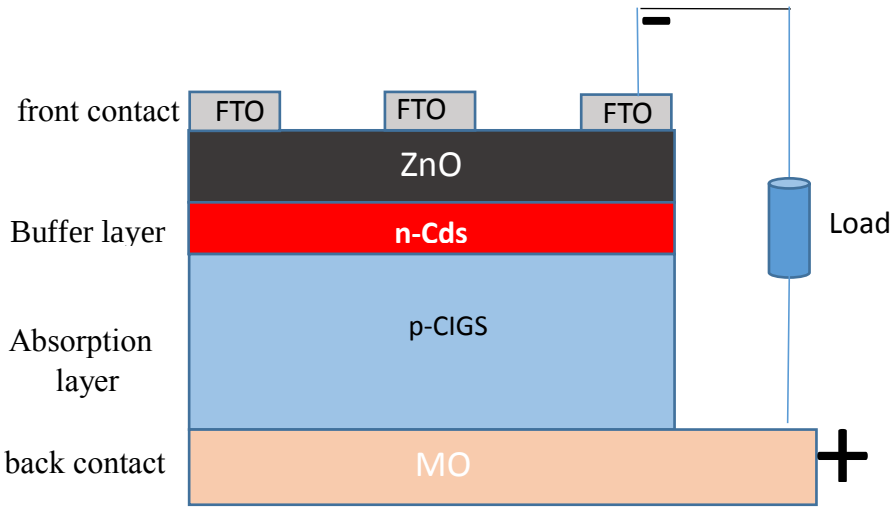

Fig III.1: Structure of CIGS-based solar cell

III.3.2.Main parameters

The physical input parameters for the modeling of $CIGS$-based PV device used in the $SCAPS$ simulation environment are presented in Table III.1.

parameter	p-CIGS	n-CdS	n-ZnO
Thickness w (μm)	varied	0.05	0.05
Bandgap Eg (eV)	1.1	2.4	3.3
Electron affinity X (eV)	4.5	4.2	4.45
Dielectric permittivity ε_r	13.6	10	9
Conduction band Nc (cm^{-3})	$2.2x10^{18}$	$2.2x10^{18}$	$2.2x10^{18}$
Valence band Nv (cm^{-3})	$1.18x10^{19}$	$1.8x10^{19}$	$1.8x10^{19}$
electron thermal velocity V_n (cm/s)	10^7	10^7	10^7
hole thermal velocity V_p (cm/s)	10^7	10^7	10^7
Electron mobility μ_e (cm^2/Vs)	100	100	100
Hole mobility μ_p (cm^2/Vs)	25	25	25
Shallow donor density ND(cm^{-3})	1	10^{17}	10^{17}
Shallow acceptor density NA(cm^{-3})	2×10^{16}	1	1
Capture cross section of electron and hole Σ (cm^2)	$5x10^{-13}$ 10^{-15}	10^{-13}	10^{-12}

Table III.1: Simulation parameters of CIGS based solar cell.

Optical absorption of the CIGS, CdS and ZnO introduced in the calculation are illustrated in Fig III.2 as function of the wavelength.

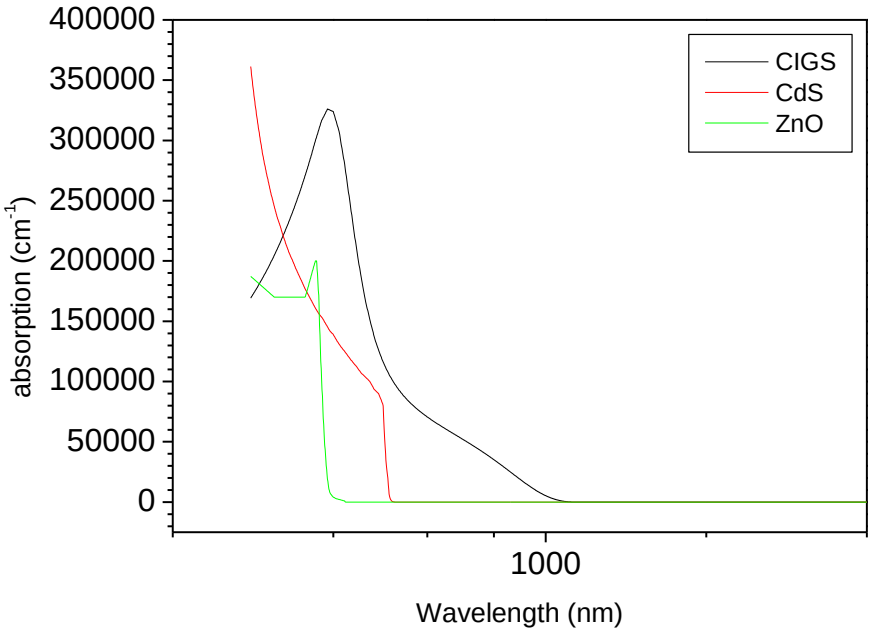

Fig III.2: optical absorption of the CIGS, CdS and ZnO

III.3.3.Effect of CIGS thickness

In order to study the effect of the thickness of the absorber layer (CIGS), we varied the thickness from 0.5 µm to 28 µm and plotted the main characteristics of the cell response in light. Fig. III.3 shows the characteristic curve (J-V) of the CIGS-based cell for different CIGS thicknesses. We observe a significant change of the I-Vcurves with the thickness of CIGS.

Fig.III.4 shows the evolution of the main characteristic parameters of the J-V curve (V_{0C}, J_{SC}, *FF* and eta) versus the CIGS thickness. We can see clearly from Fig.III.4 that all this four parameters increase rapidly with the increase of the thickness up to approximately 10 µm. Beyond this thickness these parameters reach their maximum or saturation values, ~35 mA/cm^2 , ~ 0.63 V, ~ 18.4 % and ~ 81.6 % for *Jsc*, V_{0C}, *FF* and eta, respectively.

So the maximum performance of the cell is 18.4 % which can be obtained for a minimum thickness of about 10 µm. Even if we increase the thickness further beyond this value we don't obtain an increase in the performance. This might be explained by the fact that the electrons-

holes produced by light far from the p-n junction of the solar cell are unlikely to be separated and will recombine before that.

As a conclusion, the optimum thickness value for CIGS is ~ 10 µm.

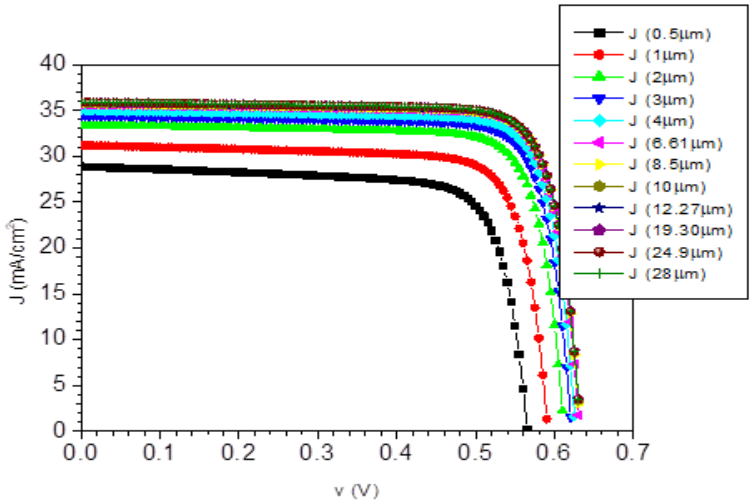

Fig III.3: The J-V curve

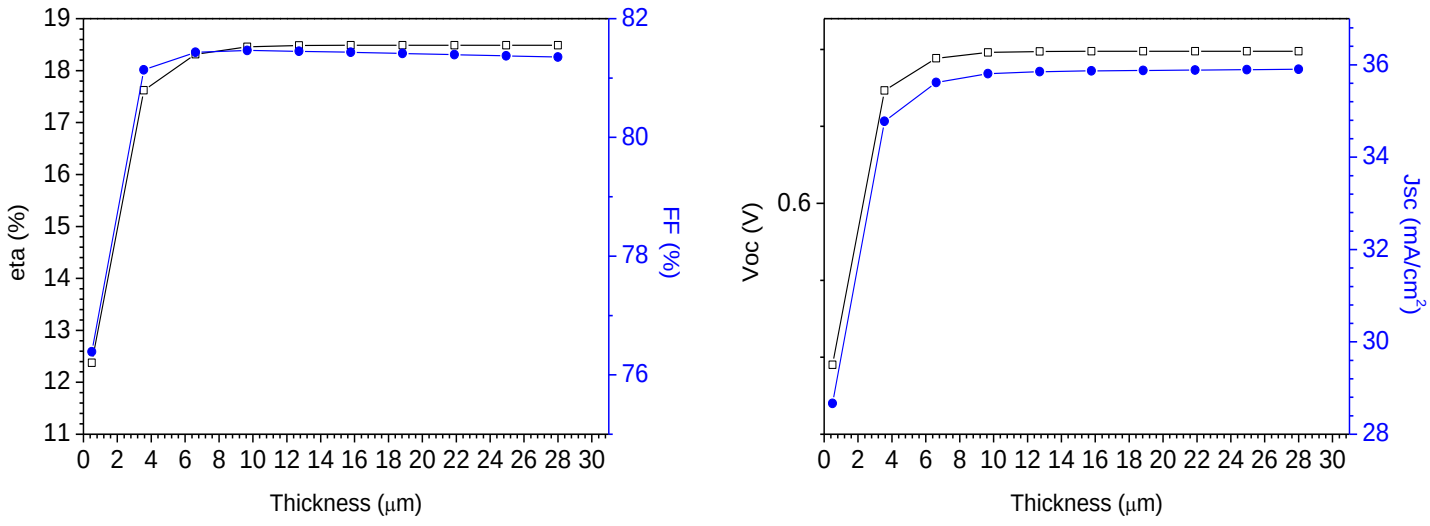

Fig III.4: The evolution versus Thickness of (a) efficiency (eta) and fill factor (FF), (b) open circuit voltage (Voc) and short circuit current (Jsc)

Similarly, in the following sections, we will explore also the impact of temperature and doping concentration on the cell parameters and plot the characteristic parameters of the J-V curve versus these variables.

III.3.4.Effect of temperature

We simulated the impact of the cell operating temperature ranging from cold operating temperature of -20 C° up to very hot temperatures of 60 C° (in the desert) . We plotted the J-V curve parameters as in the previous section.

Fig III.5 shows J-V curve for different temperatures. Fig III.6 presents the evolution of the main characteristic parameters of the J-V curve (V_{0C}, J_{SC}, *FF* and eta) versus the operating temperature of the cell.

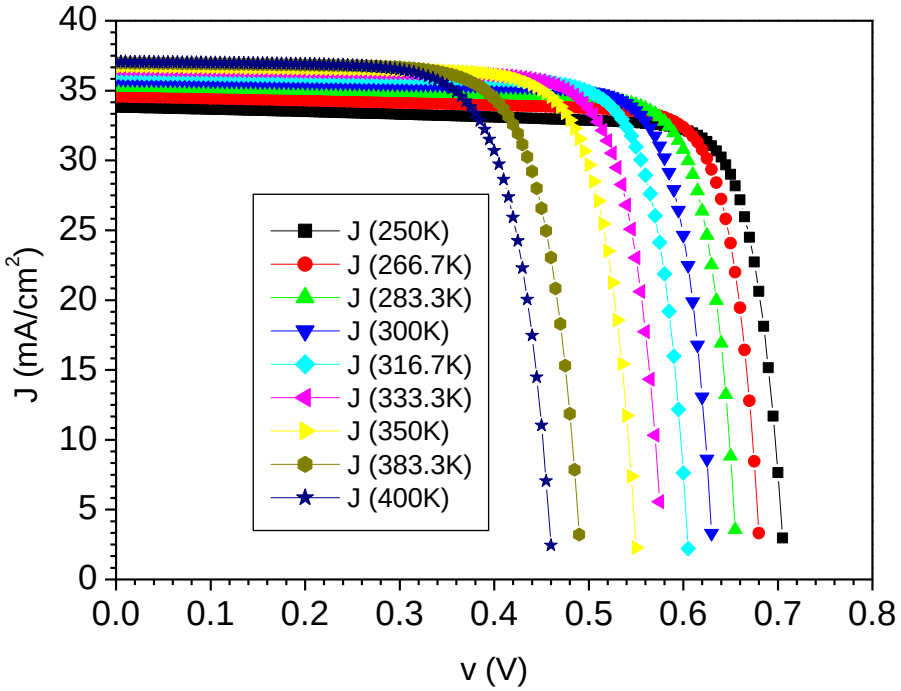

Fig III.5: The J-V curve

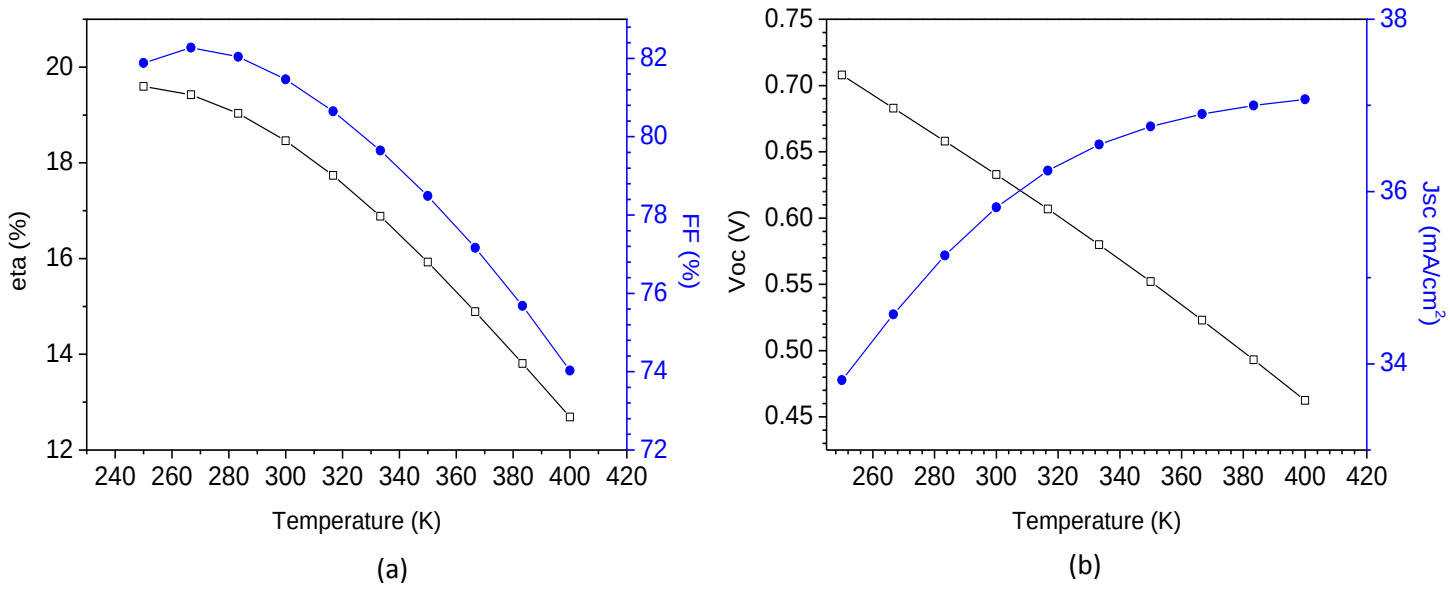

Fig III.6: The evolution versus temperature of (a) efficiency (eta) and fill factor (FF), (b) open circuit voltage (Voc) and short circuit current (Jsc)

While the short circuit current *Jsc* slightly changes from ~ 34 to 37 mA/cm^2 with the increase of temperature, the open circuit voltage V_{oc} decreases from 0.71V at 250 K to 0.46V at 400K, which leads the power conversion efficiency *eta* and the fill factor *FF* to decrease as well. The maximum values of (eta) and (FF) are obtained at the lowest temperature (250 K) and equal to 19.60% and 81.88 %, respectively, and they decrease to 12.69% and 74.03% respectively, at 400 K.

We conclude that the operating temperature affects considerably the performance of the solar cell. The lower the operating temperature, the higher the power conversion efficiency. In fact, temperature increase leads to defect concentration increase and lattice vibration to become more intense and hence the deterioration of electrical conductivity.

III.3.5.Effect of doping concentration (N_A)

We changed the concentration of acceptors from 10^{12} to 10^{17} cm^{-3} and reported the results of simulation of the *J-V* behavior of the CIGS solar cell. Fig III.7 Illustrates the evolution of the (J-V) curve versus the acceptor concentration N_A.

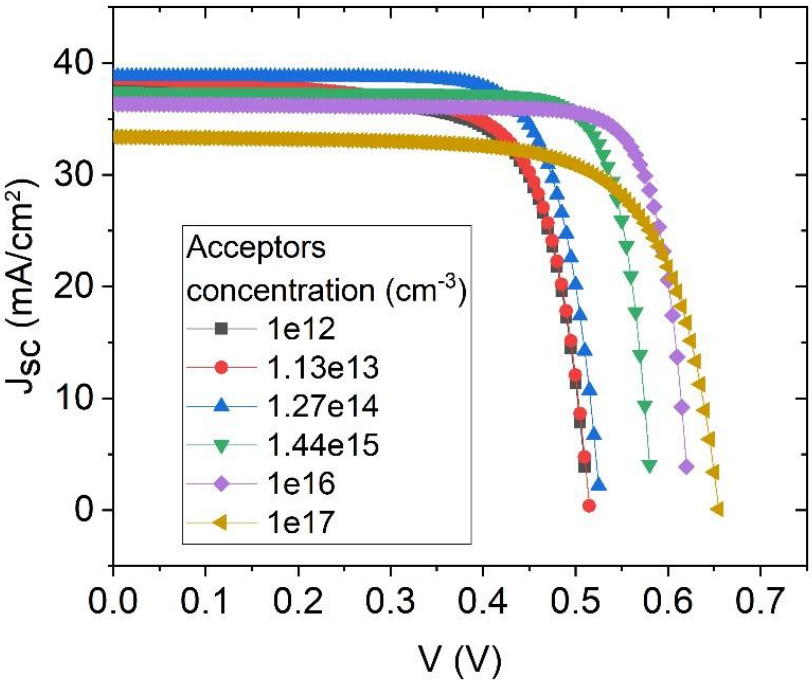

Fig III.7: The J-V curve

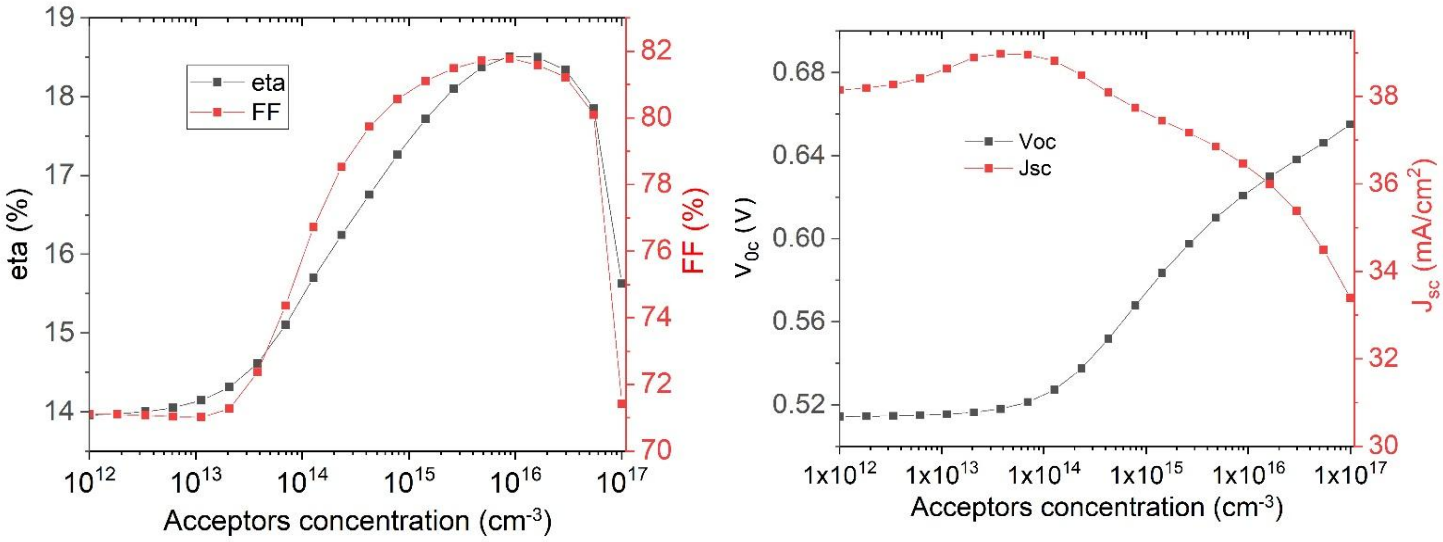

(a) (b)

Fig III.8: The evolution versus acceptors concentration of (a) efficiency (eta) and fill factor (FF), (b) open circuit voltage (Voc) and short circuit current (Jsc)

From Fig III.8, when the acceptor concentration varies from 10^{12} to ~5 $\times 10^{13}$ cm^{-3} both Voc and Jsc approximately remains constant at ~ 0.52 V and ~ 38.5 mA/cm^2, respectively. When the acceptors concentration goes beyond 5 $\times 10^{13}$ cm^{-3}, Voc increases and Jsc decreases and reach ~ 0.66 V and ~ 0.33 mA/cm^2 values, respectively, at a concentration of 10^{17} cm^{-3}. Consequently, the power conversion efficiency (eta) also remains stable (~14 %) at lower concentrations then increases with the increase of concentration and reach maximum power conversion efficiency of about 18 % for concentrations in the range from ~ 4 $\times 10^{15}$ to 2 $\times 10^{16}$ cm^{-3}. After that, further increase of the concentration up to 10^{17} cm^{-3} leads eta to decrease to values lower than 16 %.

III.3.6.Conclusion

We deduce from this optimization study, with SCAPS-1D software, of the CIGS-based solar cell that to obtain a maximum power conversion efficiency:

- The minimal CIGS thickness must be at least 10 µm.
- The acceptor concentration must be around 10^{16} cm^{-3}.
- The lower the temperature the higher the power conversion efficiency (eta).

III.4.Optimization of clathrate- Based solar cell

A new solar cell configuration that include Si allotrope called clathrate (guest-free type-II Si clathrate) has been designed and elaborated experimentally by T. Kume et al. [52]. The clathrate layer of 1 µm of thickness has been found to be an n-type semiconductor. It was deposited on a thick layer of p-type Si to form a junction. Other layers were deposited from both sides of this junction as explained in the next section to obtain the final photovoltaic device. The I-V curve was recorder experimentally and exhibited a weak photovoltaic response under white light illumination (Jsc = 9.2 nA , Voc =0.036 V and eta = 10^{-5} %). This weak response was explained by the fact that the measured resistance was very high of the order of 10^3 Ωcm^2. The authors have stated that there is a possibility of overestimation of *R* due to the inhomogeneity of the clathrate layer and the presence of an oxide layer.

Since the elaboration of clathrate layers is so costly and time consuming, we are going to optimize the parameters of this device such as the resistance, the thickness and acceptor concentration using SCAPS-1D software.

III.4.1.Configuration of the cell

The structure of the clathrate-based solar cell is comprised of the following multilayers:

ITO / Ag / **n-Si136 / p-Si** / Al.

Starting, with the ITO layer, which stands for n-type indium tin oxide. It serves as a transparent conductive electrode, allowing sunlight to penetrate into the cell and ensuring efficient light absorption. On top of the n-ITO layer, we deposit a thin layer of silver (Ag) as the contact material. This Ag layer acts as the electron collector, enabling the efficient extraction of electrons generated by the solar cell.

Next, we have the buffer layer, n-Si_{136}, an n-type silicon semiconductor. Following the n-Si_{136} layer, we deposit the p-Si layer, a p-type silicon semiconductor. This layer is responsible for absorbing photons from sunlight and generating electron-hole pairs through the photovoltaic effect. This layer forms a junction with the n-Si_{136} layer, creating a built-in electric field and facilitating the separation of charge carriers.

Finally, we introduce the Al layer, which stands for aluminum. This layer serves as the back contact of the solar cell, providing a path for the collection of the generated electrons.

Al and Ag electrodes are considered Ohmic contacts having flat-bands approach.

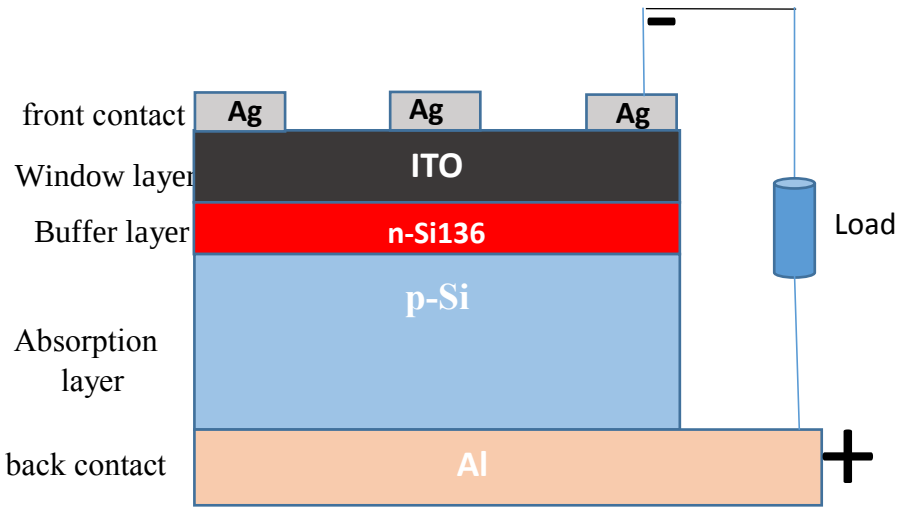

Fig III.9: Structure of clathrate-based solar cell

The structure of the simulated solar cell in this study is illustrated in Fig III.9. Additionally, the table below presents the material properties that serves as inputs to SCAPS.

III.4.2.Main parameters

The physical input parameters for the modeling of Clathrate-based *PV* device used in the *SCAPS* simulation environment are presented in Table III.2.

parameter	n-Si_{136}	p-Si
Thickness W (μm)	100	varied
Bandgap E_g (ev)	1.2	1.12
Electron affinity X (ev)	4	4.05
Dielectric permittivity	9.8	11.9
Conduction band N_c (cm^{-3})	2.58×10^{19}	2.58×10^{19}
Valence band N_v (cm^{-3})	2.65×10^{19}	2.65×10^{19}
electron thermal velocity V_n (cm/s)	10^7	10^7
hole thermal velocity V_p (cm/s)	10^7	10^7
Electron mobility μ_e (cm^2/Vs)	45	1350
Hole mobility μ_h (cm^2/Vs)	47	450
Shallow donor density ND(cm^{-3})	7×10^{20}	1
Shallow acceptor density ND(cm^{-3})	1	10^{17}
Capture cross section of electron and hole	2×10^{-14}	2×10^{-14}

Table III.2: Simulation parameters of Si_{136} based solar cell

III.4.3.Effect of n-Si 136 resistivity and thickness :

Since the resistivity of the clathrate layer depends strongly on the elaboration technique, we have performed calculations using a wide range of series resistance Rs starting from 0 Ohm (for an ideal device) up to a high value of 1500 Ohm (similar to that found by Kume et al. corresponding to inhomogeneous clathrate layer with oxide layer). We performed these calculations for three different thicknesses of the clathrate layer, 0.5, 1 and 5 µm. The result of the power conversion efficiency is reported in fig III.10.

We remark that for the ideal device (Rs = 0 Ohm), the power conversion efficiency is about 10% for a clathrate thickness of 0.5 µm. This value decreases to ~ 7% for a thickness of 1 µm and 2.5% for a thickness of 5 µm.

When the series resistance increase the eta decreases rapidly and reach a value of about 1 % when Rs ≈ 50 Ohm independently of the thickness of the clathrate layer.

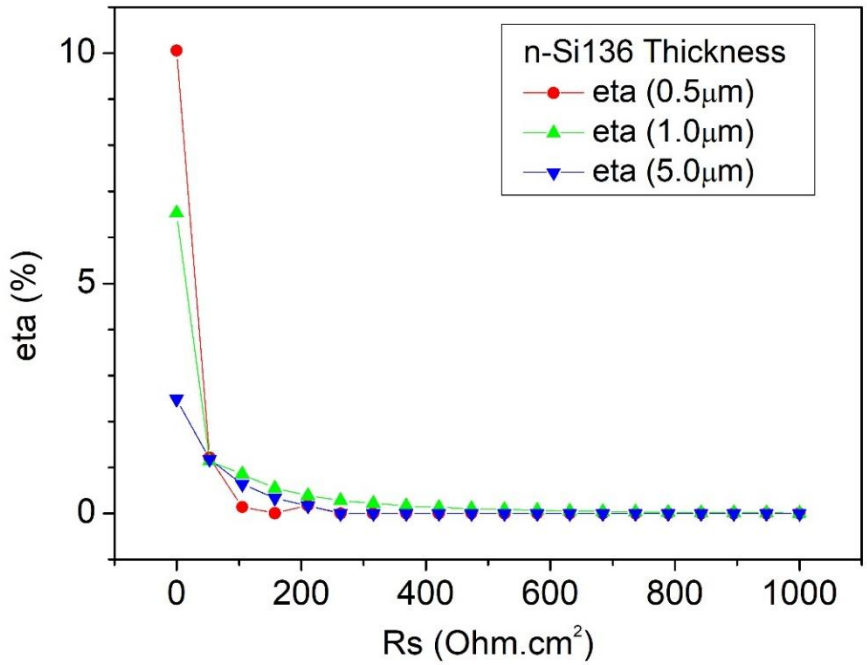

Fig III.10: Evolution of the power conversion efficiency versus the series resistance of the clathrate-based device for three different values of the clathrate thickness.

III.4.4.Effect of operating temperature

In order to check the effect of operating temperature on the power conversion efficiency, we have run the calculation code (SCAPS) for different temperatures in the usual operating

temperature, i.e. from 250 K to 400 K and plotted the Voc, Jsc, eta and FF evolution versus temperature as shown in Fig III.11.

These results were obtained for a thickness for a clathrate thickness of 1 μm and series resistance 0.5 Ohm.

When the operating temperature increases the short circuit current somewhat increases while the open circuit voltage decreases rapidly from around 0.7 to 0.35 V leading to considerable lessening of the efficiency and FF.

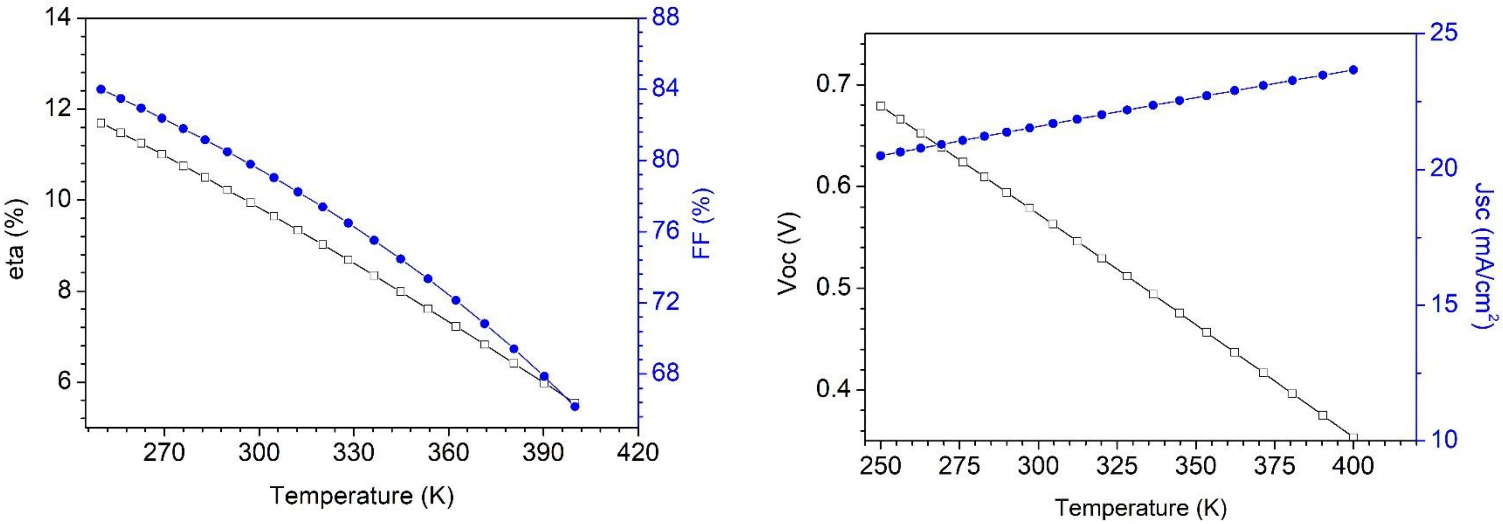

(a) (b)

Fig III.11: The evolution versus Temperature of (a) efficiency (eta) and fill factor (FF), (b) open circuit voltage (Voc) and short circuit current (Jsc)

III.4.5.Effect of the absorber layer (p-Si) thickness

Fig III.12 Shows the characteristic JV curve for different p-Si thicknesses. We plotted also Voc, Jsc, eta and FF evolution versus temperature as shown in Fig.III.13

The calculations were obtained using the optimum values of clathrate (1 μm) and Series resistance (0.5Ohm) at room temperature.

From Fig.III.13, we observe that both Voc and Jsc exhibit a weak change when the thickness of the absorber layer increase up to 35μm. After that their values reach saturation at 0.57 V and

21.6 mA/cm^2 for Voc and Jsc, respectively. Same behavior can be said for the eta and FF versus p-Si thickness. They attain their saturation values, 79.5 % and 9.7% for FF and eta respectively, beyond a p-Si thickness of around 35 µm.

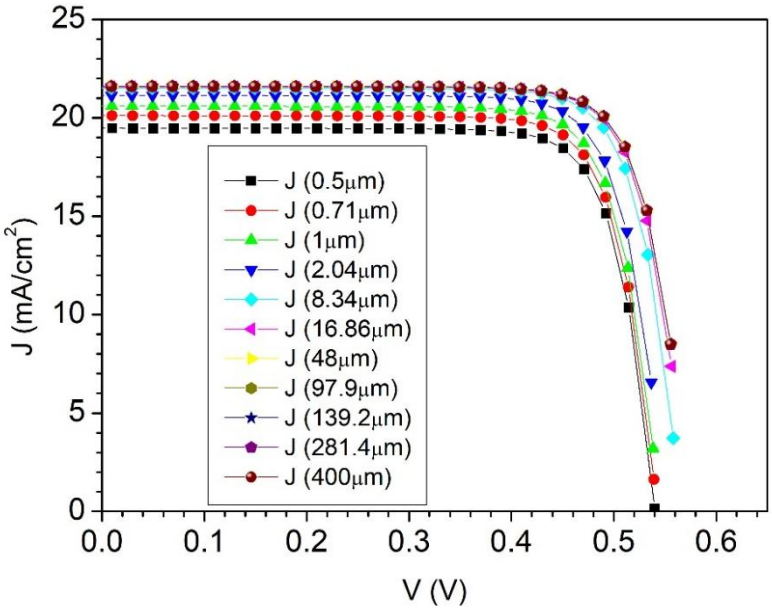

Fig III.12: The J-V curve for different p-Si layer thicknesses

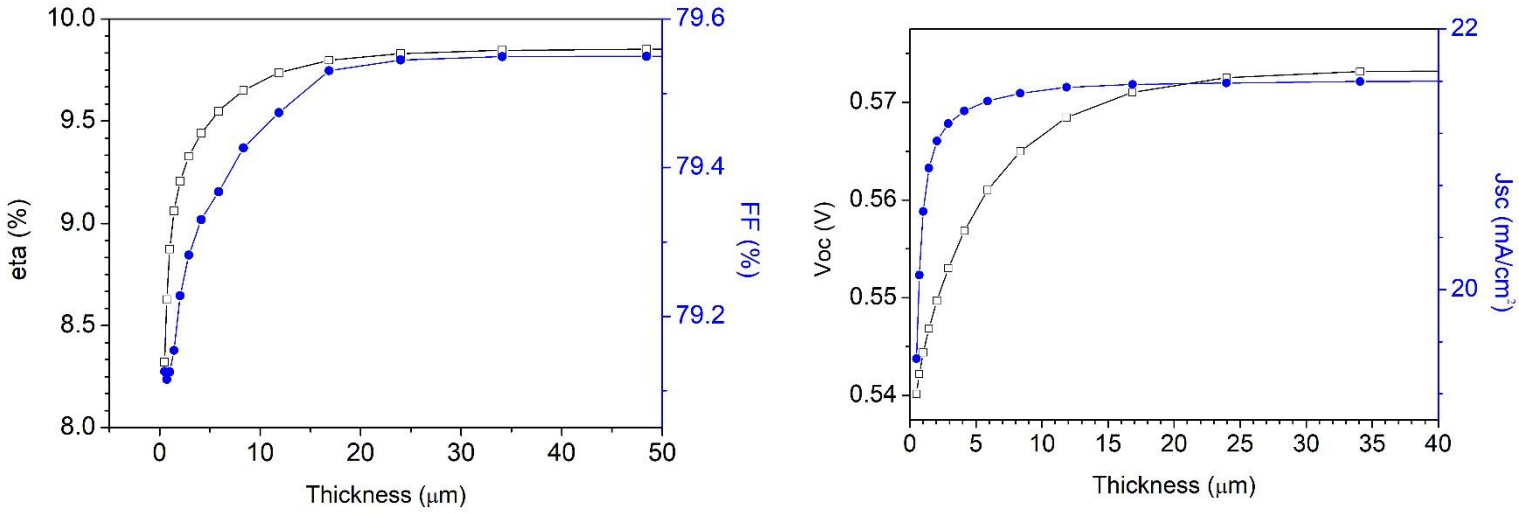

(a) (b)

Fig.III.13: The evolution versus p-Si thickness of (a) efficiency (eta) and fill factor (FF), (b) open circuit voltage (Voc) and short circuit current (Jsc)

Conclusion

Conclusion

The aim of our study was to improve the efficiency of clathrate-based solar cells, to increase their ability to convert solar energy into electrical energy with higher efficiency.

To do that, we used SCAPS-1D, a known simulation software, to study the effect of different parameters such as, layers thickness, temperature, doping concentration,…etc. We focused on the JV characteristic curve and related parameters like short circuit current *Jsc*, open circuit voltage *Voc*, fil factor *FF* and power conversion efficiency *eta* which are the main SCAPS outputs.

The simulation of the effect of different parameters on the efficiency of a CIGS standard solar cell configuration has resulted in a power conversion efficiency eta equals to 18%. This value corresponds to the following optimum parameters, an absorber tickness of 10µm and an acceptor concentration of $2x10^{16}$ cm^{-3}, however, in the simulation of the clathrate-based solar cell, with the optimization of many variables, namely, thickness, series resistance and temperature, the power conversion has attained its highest value (11.69%). This value was obtained for the following values of thickness, series resistance and temperature: 1µm, 0.5 $ohm.cm^2$ and 250K, respectively.

References

References

[1]R. Lewis, Electronics Servicing, Macmillan Education UK, London, 1983. doi:10.1007/978-1-349-05771-9.

[2] B. V Van Zeghbroeck, Principles of semiconductor devices and heterojunctions, 1st ed., Prentice Hall, 2010.

[3] https://byjus.com/physics/p-n-junction/

[4] book(Semiconductor devices Physics and technology S.M.S Z E M.K.LEE p84)

[5] https://www.iberdrola.com/social-commitment/solar-radiation

[6] MyPhD__after_revision_-2

[7] L.X.J. and F.Y.L. Fang Qin Zeng, Yan Qing Lai, Zi Li Han, Boon K. Ng, Zhi An Zhang, Hong Liang Zhang, Fabrication of earth-abundant Cu2ZnSn(S,Se)4 light absorbers by a sol–gel and selenization route for thin film solar cells, RCS Adv. 6 (2016) 6562–6570. doi:10.1039/C5RA18975F.

[8] P. Wurfel, Physics of Solar Cells from Principles to nNew Concepts, 2009. doi:10.1002/9783527618545.

[9] S.S. Li, Semiconductor Physical Electronics, Springer US, Boston, MA, 1993. doi:10.1007/978-1-4613-0489-0.

[10] F.A. Lindholm, J.G. Fossum, E.L. Burgess, Application of the superposition principle to solar-cell analysis, IEEE Trans. Electron Devices. 26 (1979) 165–171. doi:10.1109/T-ED.1979.19400.

[11] S.M. Sze, K.K. Ng, Physics of Semiconductor Devices, John Wiley & Sons, Inc., Hoboken, NJ, USA, 2006. doi:10.1002/0470068329.

[12] S.S. Li, Semiconductor Physical Electronics, Springer US, Boston, MA, 1993. doi:10.1007/978-1-4613-0489-0.

[13] H. Ullah, B. Marí, H.N. Cui, Investigation on the Effect of Gallium on the Efficiency of CIGS Solar Cells through Dedicated Software, Appl. Mech. Mater. 448–453 (2013) 1497–1501. doi:10.4028/www.scientific.net/AMM.448-453.1497.

[14] Y.H. Khattak, F. Baig, S. Ullah, B. Marí, S. Beg, H. Ullah, Numerical modeling baseline for high efficiency (Cu 2 FeSnS 4) CFTS based thin film kesterite solar cell, Optik (Stuttg). 164 (2018) 547–555.doi:10.1016/j.ijleo.2018.03.055.

[15] B. Qi, J. Wang, Fill factor in organic solar cells, Phys. Chem. Chem. Phys. 15 (2013)8972. doi:10.1039/c3cp51383a.

[16] W. Shockley, W.T. Read, Statistics of the Recombinations of Holes and Electrons, Phys. Rev. 87 (1952) 835–842. doi:10.1103/PhysRev.87.835.

[17] Using photovoltaic solar cells to produce solar electricity, (n.d.).

http://www.alternative-energy-tutorials.com/solar-power/photovoltaics.html.

[18] M.A. Green, Y. Hishikawa, W. Warta, E.D. Dunlop, D.H. Levi, J. Hohl-Ebinger, A.W.H. Ho-Baillie, Solar cell efficiency tables (version 50), Prog. Photovoltaics

[19] San-Miguel, A. and P. Toulemonde, High-pressure properties of group IV clathrates. High Pressure Research, 2005. 25(3): p. 159-185.

[20] Powell, H.M., 15. The structure of molecular compounds. Part IV. Clathrate compounds. Journal of the Chemical Society (Resumed), 1948(0): p. 61.

[21] Pauling, L. and R.E. Marsh, The Structure of Chlorine Hydrate. Proceedings of the National Academy of Sciences of the United States of America, 1952. 38(2): p. 112-118.

[22] Hiratsuka, M., et al., A molecular dynamics study of guest-host hydrogen bonding in alcohol clathrate hydrates. Physical Chemistry Chemical Physics, 2015. 17(19): p. 12639-12647.

[23] Davy, H., On a combination of oxymuriatic gas and oxygene gas. Phil. Trans. Royal.Soc. London, 1811. 155(101).

[24] M.Faraday, On Hydrate of chlorine. J. Sci, 1823. 15,71(1823).

[25] Claussen, W.F., A Second Water Structure for Inert Gas Hydrates. J Chem Phys, 1951. 19(11): p.1425-1426.

[26] Dictionary, M.-w. Clathrate. 2018 06-04-2018]; Clathrate]. Available from:https://www.merriamwebster.com/dictionary/clathrate?utm_campaign=sd&utm_medium=serp&utm_source=jsonld.

[27] Kasper, J.S., et al., Clathrate structure of silicon Na8Si46 and NaxSi136 (x< 11). Science, 1965. 150(3704): p. 1713-1714.

[28] Cros, C., M. Pouchard, and P. Hagenmuller, Sur une nouvelle famille de clathrates minéraux isotypes des hydrates de gaz et de liquides. Interprétation des résultats obtenus. Journal of Solid State Chemistry, 1970. 2(4): p. 570-581

[29] Kasper, J.S., et al., Clathrate Structure of Silicon Na₈Si₄₆ and Na_xSi₁₃₆ (x < 11) . Science, 1965. 150(3704): p. 1713-1714.

[30] Kawaji, H., et al., Superconductivity in the Silicon Clathrate Compound (Na,Ba) ${}_{\mathit{x}}$S${\mathrm{i}}_{46}$. Physical Review Letters, 1995. 74(8): p. 1427-1429.

[31] Mahammedi, N.A., M. Ferhat, and R. Belkada, Prediction of indirect to direct band gap transition under tensile biaxial strain in type-I guest-free silicon clathrate Si46: A first-principles approach. Superlattices and Microstructures, 2016. 100: p. 296-305.

References

[32] Mahammedi, N.A., M. Ferhat, and R. Belkada, Prediction of indirect to direct band gap transition under tensile biaxial strain in type-I guest-free silicon clathrate Si 46: A first-principles approach. Superlattices and Microstructures, 2016.

[33] Schäfer, M. and S. Bobev, New Type-I and Type-II Clathrates in the Systems Cs–Na–Ga–Si, Rb–Na–Ga–Si, and Rb–Na–Zn–Si. Inorganics, 2014. **2**(1): p. 79-95.

[34] Nolas, G.S., et al., Raman scattering study of stoichiometric Si and Ge type II clathrates. Journal of Applied Physics, 2002. **92**(12): p. 7225-7230.

[35] Biswas, K. and C.W. Myles, Electronic and vibrational properties of framework-substituted type-IIsilicon clathrates. Physical Review B, 2007. **75**(24).

[36] Dolyniuk, J.-A., et al., Clathrate thermoelectrics. Materials Science and Engineering: R: Reports, 2016. **108**: p. 1-46.

[37] Beekman, M., et al., Framework Contraction in Na-Stuffed Si(cF136). Inorg Chem, 2010. **49**(12): p. 5338-5340.

[38] Schafer, M.C. and S. Bobev, K and Ba distribution in the structures of the clathrate compounds KxBa16-x(Ga,Sn)136 (x = 0.8, 4.4, and 12.9) and KxBa8-x(Ga,Sn)46 (x = 0.3). Acta Crystallographica Section C, 2013. **69**(4): p. 319-323.

[39] Guloy, A.M., et al., A guest-free germanium clathrate. Nature, 2006. **443**(7109): p. 320-3.

[40] Ammar, A., et al., On the clathrate form of elemental silicon, Si136: preparation and characterization of NaxSi136 (x→0). Solid State Sciences, 2004. **6**(5): p. 393-400.

[41] Kume, T., et al., Thin film of guest-free type-II silicon clathrate on Si(111) wafer. Thin Solid Films, 2016. **609**: p. 30-34.

[42] Bobev, S. and S.C. Sevov, Clathrate III of Group 14 Exists After All. Journal of the American Chemical Society, 2001. **123**(14): p. 3389-3390.

[43] Tamegai, T., K. Uozato, and M. Tokunaga, Anisotropic superconductivity in layered silicides. Science and Technology of Advanced Materials, 2016. **7**(sup1): p. S104-S107.

[44] Mahammedi, N.A., et al., Prediction of optically-active transitions in type-VIII guest-free silicon clathrate Si46: A comparative study of its physical properties with type-I counterpart through firstprinciples. Journal of Applied Physics, 2017. **122**(20): p. 205103.

[45]M. Burgelman, P. Nollet, S. Degrave, Modelling polycrystalline semiconductor solar cells, Thin Solid Films. 361–362 (2000) 527–532. doi:10.1016/S0040-6090(99)00825-1.

[46]R.A. Jabr, M. Hamad, Y.M. Mohanna, Newton-Raphson Solution of Poisson's Equation in a Pn Diode, Int. J. Electr. Eng. Educ. 44 (2007) 23–33. doi:10.7227/IJEEE.44.1.3.

[47] Chenming C. Hu, Modern Semiconductor Devices for Integrated Circuits, in: 2010.

References

[48] O.K. Simya, A. Mahaboobbatcha, K. Balachander, A comparative study on the performance of Kesterite based thin film solar cells using SCAPS simulation program, Superlattices Microstruct. 82 (2015) 248–261. doi:10.1016/j.spmi.2015.02.020.

[49] A. Niemegeers, M. Burgelman, Numerical modelling of AC-characteristics of CdTe and CIS solar cells, in: Conf. Rec. Twenty Fifth IEEE Photovolt. Spec. Conf. - 1996, IEEE, 1996: pp. 901–904. doi:10.1109/PVSC.1996.564274.

[50] K. Decock, P. Zabierowski, M. Burgelman, Modeling metastabilities in chalcopyrite-based thin film solar cells, J. Appl. Phys. 111 (2012). doi:10.1063/1.3686651.

[51] SCAPS manual most recent

[52] T. Kume, et al., Thin film of guest-free type-II silicon clathrate on Si(111) wafer, Thin Solid Films 609 (2016) 30–34.

Abstract

A free software tool, SCAPS-1D, for simulating and modeling the performance of photovoltaic (PV) devices, has been used in the present work. It takes into account factors like material properties, device structure, and external conditions to simulate the performance characteristics of a solar cell, such as current-voltage (I-V) curves, quantum efficiency, and internal quantum efficiency. In the present work, we explored the influence of the following parameters: layer thickness, doping concentrations, series resistance and temperature on the efficiency and performance of two types of solar cells. The first one is standard CIGS-based solar cell loaded from SCAPS-1D which served as a training step. The second is a clathrate-based solar cell, a new configuration of solar cells including an n-type semiconductor layer of an allotrope of silicon called clathrate. The simulation results of the clathrate-based solar cell predicted that the power conversion efficiency might reach ~10 % using optimized p-Si and clathrate thicknesses and if a high quality clathrate layer is successfully deposited without inhomogeneity and oxide layer, i.e., with low resistivity. Therefore, this new solar cell configuration is promising and further studies of the effect of other parameters is necessary to attain higher efficiencies.

Résumé

Un logiciel gratuit, SCAPS-1D, utilisé dans cette étude, permet de simuler et de modéliser les performances des dispositifs photovoltaïques (PV). Il prend en compte des facteurs tels que les propriétés des matériaux, la structure du dispositif et les conditions externes pour simuler les caractéristiques de performance d'une cellule solaire, telles que les courbes courant-tension (I-V), l'efficacité quantique et l'efficacité quantique interne. Dans cette étude, nous avons exploré l'influence des paramètres suivants : l'épaisseur de la couche, les concentrations de dopage, la résistance série et la température sur l'efficacité et les performances de deux types de cellules solaires. Le premier est une cellule solaire à base de CIGS standard chargée à partir de SCAPS-1D, qui a servi d'étape d'entraînement. Le deuxième est une cellule solaire à base de clathrate, une nouvelle configuration de cellules solaires comprenant une couche semi-conductrice de type n d'un allotrope de silicium appelé clathrate. Les résultats de simulation de la cellule solaire à base de clathrate ont prédit que le rendement de conversion de puissance pourrait atteindre ~10 % en utilisant des épaisseurs de p-Si et de clathrate optimisées et si une couche de clathrate de haute qualité est déposée avec succès sans inhomogénéité ni couche d'oxyde, c'est-à-dire avec une faible résistivité. Par conséquent, cette nouvelle configuration de cellule solaire est prometteuse et des études supplémentaires sur l'effet d'autres paramètres sont nécessaires pour atteindre des rendements plus élevés.

ملخص

تم استخدام أداة برمجية مجانية تسمى SCAPS-1D في هذا العمل لمحاكاة ونمذجة أداء أجهزة الطاقة الشمسية . تأخذ الأداة في الاعتبار عوامل مثل خصائص المواد وهيكل الجهاز والظروف الخارجية لمحاكاة خصائص الأداء لخلية شمسية، مثل منحنيات التيار-الجهد (I-V) وكفاءة الكم وكفاءة الكم الداخلية. في هذا العمل، استكشفنا تأثير العوامل التالية: سمك الطبقة، تراكيز التنشيط، المقاومة التسلسلية ودرجة الحرارة على الكفاءة والأداء لنوعين من خلايا الطاقة الشمسية. النوع الأول هو خلية شمسية قائمة على CIGS تم تحميلها من SCAPS-1D والتي تعمل كخطوة تدريبية. النوع الثاني هو خلية شمسية قائمة على الكلاتريت، وهي تكوين جديد لخلايا الطاقة الشمسية يتضمن طبقة نصف موصلة من نوع n مصنوعة من السيليكون المتاصل يُسمى الكلاتريت. أظهرت نتائج المحاكاة للخلية الشمسية القائمة على الكلاتريت أن كفاءة تحويل الطاقة يمكن أن تصل إلى حوالي 10% باستخدام سماكات محسّنة للسيليكون نوع p والكلاتريت، وإذا تمكنا من وضع طبقة كلاتريت عالية الجودة بدون تشوهات أو طبقة أكسيد، أي بمقاومة منخفضة. وبالتالي، فإن تكوين خلية الطاقة الشمسية الجديد هذا واعد ويتطلب دراسات إضافية لتحديد تأثير العوامل الأخرى على الكفاءة لتحقيق كفاءات أعلى.